Journal of the Mechanics and Physics of Solids 57 (2009) 342–368

Contents lists available at ScienceDirect

Journal of the Mechanics and Physics of Solids

journal homepage: www.elsevier.com/locate/jmps

Laws of crack motion and phase-field models of fracture

Vincent Hakim [a,*], Alain Karma [b]

[a] Laboratoire de Physique Statistique, CNRS-UMR8550 associé aux universités Paris VI et VII, Ecole Normale Supérieure, 24 rue Lhomond, 75231 Paris, France
[b] Physics Department and Center for Interdisciplinary Research on Complex Systems, Northeastern University, Boston, MA 02115, USA

ARTICLE INFO

Article history:
Received 4 June 2008
Received in revised form
18 October 2008
Accepted 21 October 2008

PACS:
62.20.Mk
46.50+a
46.15.−x

Keywords:
Fracture
Phase field
Anisotropy
Eshelby tensor
Herring torque

ABSTRACT

Recently proposed phase-field models offer self-consistent descriptions of brittle fracture. Here, we analyze these theories in the quasistatic regime of crack propagation. We show how to derive the laws of crack motion either by using solvability conditions in a perturbative treatment for slight departure from the Griffith threshold or by generalizing the Eshelby tensor to phase-field models. The analysis provides a simple physical interpretation of the second component of the classic Eshelby integral in the limit of vanishing crack propagation velocity: it gives the elastic torque on the crack tip that is needed to balance the Herring torque arising from the anisotropic surface energy. This force-balance condition can be interpreted physically based on energetic considerations in the traditional framework of continuum fracture mechanics, in support of its general validity for real systems beyond the scope of phase-field models. The obtained law of crack motion reduces in the quasistatic limit to the principle of local symmetry in isotropic media and to the principle of maximum energy-release-rate for smooth curvilinear cracks in anisotropic media. Analytical predictions of crack paths in anisotropic media are validated by numerical simulations. Interestingly, for kinked cracks in anisotropic media, force-balance gives significantly different predictions from the principle of maximum energy-release-rate and the difference between the two criteria can be numerically tested. Simulations also show that predictions obtained from force-balance hold even if the phase-field dynamics is modified to make the failure process irreversible. Finally, the role of dissipative forces on the process zone scale as well as the extension of the results to motion of planar cracks under pure antiplane shear are discussed.

1. Introduction

The prediction of the path chosen by a crack as it propagates into a brittle material is a fundamental problem of fracture mechanics. It has classically been addressed in a theoretical framework where the equations of linear elasticity are solved with zero traction boundary conditions on crack surfaces that extend to a sharp tip (Broberg, 1999). In this description, the stress distributions near the crack tip have the universal divergent forms (William, 1957; Irwin, 1957)

$$\sigma_{ij}^{m}(r,\Theta)=\frac{K_m}{\sqrt{2\pi r}}f_{ij}^{m}(\Theta), \tag{1}$$

* Corresponding author.
E-mail address: hakim@lps.ens.fr (V. Hakim).

0022-5096/$ - see front matter © 2008 Elsevier Ltd. All rights reserved.
doi:10.1016/j.jmps.2008.10.012

where K_m are the stress intensity factors (SIF) for the three standard modes I, II, or III of fracture ($m = 1, 2$ or 3), Θ is the angle between the radial vector of magnitude r with origin at the crack tip and the local crack direction and the explicit expressions of the f_{ij}'s are recalled in Appendix C (see Eq. (C.4)). The allied energy-release-rate (or crack extension force) reads, for plane strain,

$$G = \alpha(K_1^2 + K_2^2) + K_3^2/(2\mu), \tag{2}$$

where ν denotes Poisson's ratio, μ is the shear modulus, and $\alpha \equiv (1-\nu)/(2\mu)$. Following Griffith (1920), Irwin (1957) postulated that for the crack to propagate, G must exceed some material-dependent threshold G_c that is theoretically equal to twice the surface energy ($G_c = 2\gamma$), but often larger in practice. Griffith's theory provide one criterion for crack propagation but is insufficient to determine curvilinear crack paths or crack kinking and branching angles. Like other problems in fracture, the prediction of the crack direction of propagation was first examined (Barenblatt and Cherepanov, 1961) for mode III which is simpler because the antiplane component of the displacement vector u_3 is a purely scalar Laplacian field. In this case, the stress distribution near the tip, can be expanded as

$$\sigma_{3\Theta} \equiv \frac{\mu}{r}\frac{\partial u_3}{\partial \Theta} = \frac{K_3}{\sqrt{2\pi r}}\cos\frac{\Theta}{2} - \mu A_2 \sin\Theta + \cdots. \tag{3}$$

The dominant divergent contribution is always symmetrical about the crack direction. As a consequence, the knowledge of K_3 alone cannot predict any other path than a straight one. To avoid this impasse, Barenblatt and Cherepanov (1961) retained the subdominant $\sin\Theta$ term, which breaks this symmetry. They hypothesized that a curvilinear crack propagates along a direction where $A_2 = 0$, when the stress distribution is *symmetrical* about the crack direction. In subsequent extensions of this work, several criteria have been proposed for plane loading, for which the tensorial nature of the stress fields makes it possible to predict non-trivial crack paths purely from the knowledge of the SIFs (Goldstein and Salganik, 1974; Cotterell and Rice, 1980). The generally accepted condition "$K_2 = 0$" assumes that the crack propagates in a pure opening mode with a symmetrical stress distribution about its local axis (Goldstein and Salganik, 1974) and is the direct analog for plane strain ($u_3 = 0$) of the condition $A_2 = 0$ for mode III. This "principle of local symmetry" has been rationalized using plausible arguments (Cotterell and Rice, 1980) in the classical framework of fracture mechanics. It has also been argued to follow from continuity of the chemical potential at the fracture tip, in a model that incorporates surface diffusion (Brener and Marchenko, 1998). A full derivation requires an explicit description of the process zone, where elastic strain energy is both dissipated and transformed nonlinearly into new fracture surfaces. As a result, how to extend this principle to anisotropic materials, where symmetry considerations have no obvious generalization, is not clear (Marder, 2004a). This is also the case for curved three-dimensional fractures although this appears little-noted in the literature. In addition, path prediction remains largely unexplored for mode III even for isotropic materials.

Continuum models of brittle fracture that describe both short scale failure and macroscopic linear elasticity within a self-consistent set of equations have recently been proposed (Aranson et al., 2000; Karma et al., 2001; Eastgate et al., 2002; Wang et al., 2002; Marconi and Jagla, 2005; Spatschek et al., 2006). These models have already shown their usefulness in various numerical simulations. For both antiplane (Karma and Lobkovsky, 2004) and plane (Henry and Levine, 2004) loading, they have proven capable to reproduce the onset of crack propagation at Griffith threshold as well as dynamical branching (Karma and Lobkovsky, 2004; Henry, 2008) and oscillatory (Henry and Levine, 2004) instabilities. In a quasistatic setting, this continuous media approach differs in spirit but has nonetheless much in common with a variational approach to brittle fracture (Francfort and Marigo, 1998) proposed to overcome limitations of Griffith theory. This is especially apparent when the latter is implemented numerically (Bourdin et al., 2000), using ideas (Ambrosio and Tortorelli, 1990) initially developed for image segmentation (Mumford and Shah, 1989).

In this article, we analyze these self-consistent theories of brittle fracture for mode I/II cracks as well as for cracks moving under pure antiplane shear (mode III) and show how to *derive* laws of motion for the crack tip. This provides, in particular, relations which generalize the principle of local symmetry for an anisotropic material. Furthermore, we validate these relations by phase-field simulations. This validation is carried out both for the traditional variational formulation of the phase-field model with a so-called "gradient dynamics", which guarantees that the total energy of the system, i.e. the sum of the elastic and cohesive energies, decreases monotonously in time, and for a simple modification of this dynamics that makes the failure process irreversible. We find that both formulations yield essentially identical crack paths that are well predicted by the laws of crack motion derived from the phase-field model.

In isotropic media, the principle of local symmetry and the principle of maximum energy-release-rate gives identical prediction for smooth curvilinear cracks and very small differences for kinked angles (see e.g. Cotterell and Rice, 1980; Hutchinson and Suo, 1992; Amestoy and Leblond, 1992). This makes it difficult to numerically distinguish these two criteria. Thus, for kinked cracks, it has remained somewhat unclear what happens for stresses in the gap above the maximum energy-release-rate threshold stress (where energetic considerations alone appear to require crack propagation) but below the minimal stress where propagation with local symmetry/force-balance is possible. Interestingly, we find that the force-balance and maximum energy-release-rate principles can give significantly distinct predictions in anisotropic media for some choices of surface energy anisotropy and loading conditions. Numerical simulations, which are at the limit of what is computationally feasible with a finite-difference implementation of the phase-field equations on a regular mesh, show that kink cracks emerge from the main crack tip at an initial angle, which appears close to the one predicted by

maximum energy-release-rate, and turn on the process zone length scale towards the angle predicted by force-balance for straight kinks.

For clarity of exposition, the relations derived from the phase-field model are summarized first in Section 2 and interpreted physically in the context of previous results from the fracture community. This section stresses why the second component of the Eshelby configurational force perpendicular to the crack axis is both physically meaningful and important for the determination of crack paths.

Our approach is applicable to a large class of diffuse interface descriptions of brittle fracture. However, for clarity of exposition, we base our derivation on the phase-field model introduced by Karma et al. (2001). As recalled in Section 3, in this description, the displacement field is coupled to a single scalar order parameter or "phase-field" ϕ, which describes a smooth transition in space between unbroken ($\phi = 1$) and broken states ($\phi = 0$) of the material. We focus on quasistatic fracture in a macroscopically isotropic elastic medium with negligible inertial effects. Material anisotropy is simply included by making the surface energy $\gamma(\theta)$, dependent on the orientation θ of the crack direction with respect to some underlying crystal axis. In Section 4, we analyze the quasistatic motion of a crack propagating in mode I/II, perturbatively for small departure from Griffith threshold ($|G - G_c|/G_c \ll 1$) and small anisotropy. The crack laws of motion are shown to be determined in a usual manner by solvability conditions, coming from translation invariance parallel and perpendicular to the crack tip axis. A different derivation is provided in Section 5 by generalizing Eshelby (1975) tensor to phase-field theories. The relation and differences between force-balance and maximum energy-release-rate criteria are then considered. The particular case of motion under pure antiplane shear is discussed in Section 6. Our analytical predictions are compared with numerical phase-field simulations in Section 7 where we also examine the sensitivity of the results to the irreversibility of the failure process. Our conclusions and some further perspectives of this work are then presented in Section 8. Further information on the phase-field model of Karma et al. (2001) is provided in Appendix A in the simple context of a stretched one-dimensional band. Details of some of our calculations are provided in Appendices B and C. A short version of this work has been published in Hakim and Karma (2005).

2. An overview of the physical picture and main results in the classical fracture formalism

In the formalism of continuum fracture mechanics, crack propagation has been traditionally analyzed by considering the crack extension force G defined by Eq. (2). This is a purely configurational force that points along the crack axis in the direction of propagation where $G\delta l$ is the amount elastic energy released when the crack advances infinitesimally along this axis by a distance δl. When considering the propagation of a general curvilinear crack, however, it is necessary to consider the extension of a crack at some small infinitesimally angle $\delta\theta$ with respect to its current axis as depicted schematically in Fig. 1. Physically, one would expect a configurational force, distinct from G, to be associated with the extra amount of elastic energy that is released if the crack propagates by δl along this new direction, denoted here by $\hat{t}$, as opposed to propagating the same distance along its current axis, denoted by $\hat{x}_1$.

This additional force on the crack tip was considered by Eshelby (1975). It can be interpreted physically as producing a torque on the crack tip that changes the crack propagation direction so as to maximize the elastic energy released. The force that produces this torque must act perpendicularly to the crack propagation direction and its magnitude is simply

$$G_\theta \equiv \lim_{\delta\theta\to 0} \frac{\delta G}{\delta\theta}, \tag{4}$$

where δG is the difference between the crack extension force along the new direction and the old direction, i.e. along $\hat{t}$ and $\hat{x}_1$ in Fig. 1. This torque is analogous to the well-known "Herring (1951, p. 143) torque" acting on the junction of three crystal grains of different orientations in a polycrystalline material, with the main difference that G_θ is a configurational force in the present fracture context while the Herring torque is produced by a physical force associated with the grain boundary energy, $\gamma_{gb}(\theta)$, which is generally anisotropic. This force acts perpendicularly to each grain boundary segment at the junction of three grains with a magnitude $\mathrm{d}\gamma_{gb}/\mathrm{d}\theta$.

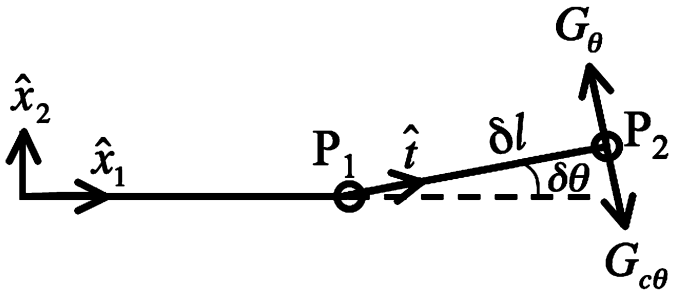

Fig. 1. Schematic representation of an infinitesimal extension P_1P_2 of the crack of length δl at and angle $\delta\theta$ measured with respect to the crack axis. The arrows pointing perpendicular to the crack denote the two analogs G_θ and $G_{c\theta}$ of the Herring torque associated with the directional dependence of the crack extension force and the fracture energy around the crack axis, respectively.

This analogy suggests that there should generally be two torques acting on the crack tip. The first, already mentioned, is Eshelby's configurational elastic torque G_θ associated with the directional dependence of the crack extension force in reference to the local crack axis. The second is the physical torque associated with the directional dependence of the fracture energy, defined here by $G_c(\theta)$, which should have a magnitude $\mathrm{d}G_c(\theta)/\mathrm{d}\theta \equiv G_{c\theta}$ by direct translation of Herring's result for fracture. It follows that the balance of forces at the crack tip should yield two conditions. The first is the standard condition of the classical fracture formalism associated with the balance of forces along the crack axis, $G = G_c$. The second is the condition

$$G_\theta = G_{c\theta} = 2\gamma_\theta, \tag{5}$$

which corresponds physically to the balance of the two aforementioned torques acting on the crack tip. While G_θ pulls the crack in a direction that tends to maximize the release of elastic energy, $G_{c\theta}$ pulls the crack in a direction that minimizes the energy cost of creating new fracture surfaces. The second equality on the right-hand side (r.h.s.) of Eq. (5) only holds in some ideal brittle limit where the fracture energy is equal to twice the surface energy, defined here by $\gamma(\theta)$, and $\gamma_\theta \equiv \mathrm{d}\gamma(\theta)/\mathrm{d}\theta$. We note that this ideal brittle limit is exact for the class of phase-field models analyzed in this paper but at best only approximate even for a strongly brittle material such as glass. The issue of the quantitative evaluation of $G_{c\theta}$, however, should be kept separate from its role in crack path prediction that is our main focus in this paper.

To see how this torque balance condition provides an explicit prediction for the crack path, it is useful to derive an expression for G_θ by elementary means, directly from the definition of Eq. (4), instead of by evaluating an Eshelby–Rice type integral around the crack tip (Rice, 1968; Eshelby, 1975), as done later in this paper (see Section 5 and Appendix C); while both methods yield the same answer, the former is more physically transparent. For this purpose, we use the known expressions for the new SIFs $\tilde{K}_1$ and $\tilde{K}_2$ at the tip (corresponding to P_2 in Fig. 1) of an infinitesimally small kink extension of length δl of a semi-infinite crack (Amestoy and Leblond, 1992). In the limit of vanishing kink angle, these expressions are given by

$$\tilde{K}_1 = K_1 - 3K_2\delta\theta/2 + \cdots, \tag{6}$$

$$\tilde{K}_2 = K_2 + K_1\delta\theta/2 + \cdots \tag{7}$$

to linear order in $\delta\theta$ independently of δl, where K_1 and K_2 are the SIFs at the tip (corresponding to P_1 in Fig. 1) of the original straight crack. Using Eq. (2) with these new SIFs to define $G(\delta\theta)$, we obtain at once that $\delta G = G(\delta\theta) - G(0) = -2\alpha K_1 K_2 \delta\theta$, and hence using Eq. (4), that $G_\theta = -2\alpha K_1 K_2$. Substituting this expression for G_θ in the torque balance condition (5), we obtain the condition

$$K_2 = -\frac{G_{c\theta}}{2\alpha K_1} = -\frac{\gamma_\theta}{\alpha K_1}, \tag{8}$$

where second equality only holds in the ideal brittle limit as before. In the isotropic limit where $G_{c\theta}$ vanishes, this condition reduces to the principle of local symmetry which assumes that the crack propagates in a pure opening mode ($K_2 = 0$). In contrast, for an anisotropic material, K_2 is finite with a magnitude that depends both on K_1 and the local crack propagation direction, i.e. $G_{c\theta}$ depends on the direction of the crack with respect to some fixed crystal axis in a crystalline material. For simplicity, we have restricted our derivation to a situation where linear elasticity is isotropic (e.g. hexagonal symmetry in two dimensions), but Eq. (8) could straightforwardly be extended to a more general situation where linear elasticity is also anisotropic.

The recognition that the torque balance condition (5) can be used to determine the general path of a crack in a brittle material is the central result of this paper. This condition sheds light on the physical origin of the principle of local symmetry in the isotropic limit and shows how it can be generalized quantitatively to anisotropic materials. Although the configurational force perpendicular to the crack tip was considered explicitly by Eshelby (1975) it has been largely ignored until recently. This is perhaps because the displacement of a small segment of crack perpendicular to itself, which one might naively expect to result from such a force, would appear unphysical and unreconcilable with the irreversibility of the fracture process. While such a motion is unphysical, it should be clear from the present considerations that all the torques acting on the crack tip, both the elastic configurational torque G_θ and the physical torque $G_{c\theta}$ linked to fracture energy anisotropy, have been obtained solely from the consideration of an infinitesimal, physically admissible, extension of the crack at a small angle from its axis. In equating these two torques at the crack tip, the main assumption made is that the dynamics on the process zone scale is able to sample different possible microscopic states so as to permit local relaxation to mechanical equilibrium.

There have been more recent attempts to incorporate the Eshelby elastic torque in the classical fracture formalism, where fracture surfaces are treated as mathematically sharp boundaries extending to the crack tip (Adda-Bedia et al., 1999; Oleaga, 2001; Marder, 2004a). In particular, based on energetic considerations, Marder (2004b) has proposed an equation of motion that reduces to Eq. (8) for smooth curvilinear cracks, albeit not for kinked cracks, in the limit when a phenomenologically introduced relaxation length scale (Hodgdon and Sethna, 1993) vanishes. In the context of these previous studies, the phase-field approach has the important advantage of removing many of the ambiguities that arise when considering the motion of the crack tip in the classical fracture formalism. In particular, it makes it possible to

rigorously derive a force (torque) balance condition from the condition for the existence of a propagating crack solution that is spatially diffuse on the inner scale of the process zone and that must match smoothly to the standard solution of linear elasticity on the outer scale of the sample size. This condition reduces to Eq. (5) (or Eq. (8) for isotropic elasticity) in the limit of vanishing crack velocity. Furthermore, it holds generally for both smooth and kinked cracks and predicts kink angles that differ from those predicted by maximum energy-release-rate. Furthermore, this force-balance condition contains additional contributions for finite crack velocity associated with dissipative forces on the process zone scale.

Interestingly, the results of the phase-field analysis show that the component of the dissipative force perpendicular to the crack tip vanishes for propagation in isotropic media because both the stress distribution and the phase field are symmetrical about the crack axis in this case. Consequently, within the phase-field framework, dissipative forces do not change the condition $K_2 = 0$ for crack propagation in isotropic media. For propagation in anisotropic media, in contrast, small velocity-dependent correction to the torque balance condition (8) arise because this symmetry is broken.

3. The KKL phase-field model of fracture

Fracture is generally described in diffuse interface models (Aranson et al., 2000; Karma et al., 2001; Eastgate et al., 2002; Wang et al., 2002; Marconi and Jagla, 2005) as a softening of the elastic moduli at large strains. This can be done purely in term of the strain tensor but it produces field equations with derivative of high order (Marconi and Jagla, 2005). Here, we adopt the alternative approach of introducing a supplementary field ϕ, a scalar order parameter or "phase field", that describes the state of the material and smoothly interpolates between intact ($\phi = 1$) and fully broken ($\phi = 0$) states. For definiteness, we base our derivation on the specific model proposed by Karma et al. (2001) with energy density $\mathscr{E}$,

$$\mathscr{E} = \mathscr{E}_{pf}(\{\partial_j\phi\}) + g(\phi)(\mathscr{E}_{strain} - \mathscr{E}_c) + \mathscr{E}_c, \tag{9}$$

where $\partial_j \equiv \partial/\partial x_j$ denotes the partial derivative with respect to the cartesian coordinate x_j ($j = 1,2,3$) and $\mathscr{E}_{strain}$ is the elastic energy of the intact material. The equations of motion are derived variationally from the total energy of the system that is the spatial integral

$$E = \int \mathrm{d}^3x\, \mathscr{E} \tag{10}$$

of the energy density. In the quasistatic case, these are

$$0 = -\frac{\delta E}{\delta u^k} = \partial_j \frac{\partial \mathscr{E}}{\partial[\partial_j u^k]} - \frac{\partial \mathscr{E}}{\partial u^k}, \tag{11}$$

$$\chi^{-1}\partial_t\phi = -\frac{\delta E}{\delta \phi} = \partial_j \frac{\partial \mathscr{E}}{\partial[\partial_j \phi]} - \frac{\partial \mathscr{E}}{\partial \phi}. \tag{12}$$

The three Euler–Lagrange equation (11) for the cartesian components u_k of the displacement vector ($k = 1,2,3$) are simply the static equilibrium conditions that the sum of all forces on any material element vanish. The fourth equation (12) for ϕ is the standard Ginzburg–Landau form that governs the phase-field evolution, with χ a kinetic coefficient that controls the rate of energy dissipation in the process zone, i.e. it follows from Eqs. (11) and (12) that

$$\frac{\mathrm{d}E}{\mathrm{d}t} = -\chi \int \mathrm{d}^3x \left(\frac{\delta E}{\delta \phi}\right)^2 \leqslant 0. \tag{13}$$

In the simplest case of an isotropic elastic medium and isotropic ϕ, the phase field and strain energy are simply

$$\mathscr{E}_{pf}(\{\partial_j\phi\}) = \frac{\kappa}{2}(\nabla\phi)^2, \tag{14}$$

$$\mathscr{E}_{strain}(\{u_{ij}\}) = \frac{\lambda}{2}(u_{ii})^2 + \mu u_{ij}u_{ij}, \tag{15}$$

where $u_{ij} = (\partial_i u_j + \partial_j u_i)/2$ is the usual strain tensor of linear elasticity. No asymmetry between dilation and compression is included since this is not necessary for our present purposes. The broken state of the material becomes energetically favored when $\mathscr{E}_{strain}$ exceeds the threshold $\mathscr{E}_c$ and $g(\phi)$ is a monotonically increasing function of ϕ that describes the softening of the elastic energy at large strain ($g(0) = 0$) and produces the usual elastic behavior for the intact material ($g(1) = 1, g'(1) = 0$). In addition, the release of bulk stress by a crack requires the function $g(\phi)$ to vanish faster than ϕ^2 for small ϕ, as recalled in Appendix A. We therefore choose $g(\phi) = 4\phi^3 - 3\phi^4$, as in Karma et al. (2001), Karma and Lobkovsky (2004), and Henry and Levine (2004). With these choices, the isotropic surface energy is equal to

$$\gamma_0 = \sqrt{2\kappa\mathscr{E}_c}\int_0^1 \mathrm{d}\phi\sqrt{1 - g(\phi)} \simeq 0.7165\sqrt{2\kappa\mathscr{E}_c}, \tag{16}$$

as shown in Appendix A (Eq. (A.22)), by repeating the analysis of Karma et al. (2001).

In the present paper, we analyze the case of a phase-field energy $\mathscr{E}_{pf}(\{\partial_j\phi\})$ without rotational symmetry which gives an anisotropic surface energy. A simple example used for concreteness and for the numerical simulations is provided by a simple two-fold anisotropy in the phase-field energy[1]

$$\mathscr{E}_{pf} = \frac{\kappa}{2}(|\nabla\phi|^2 + \varepsilon\partial_1\phi\partial_2\phi). \tag{17}$$

The surface energy of a straight fracture interface oriented at an angle θ with the x-axis arises from the variation of the elastic and phase fields in a direction transverse to the fracture, namely with $\phi(x,y) = \phi[-x\sin(\theta) + y\cos(\theta)]$. Therefore, the only difference between Eqs. (14) and (17) in this one-dimensional calculation of the surface energy (Appendix A) is the replacement of κ by $\kappa[1-(\varepsilon/2)\sin 2\theta]$ in the anisotropic case. The allied anisotropic surface energy thus follows directly from the isotropic expression (16) and reads

$$\gamma(\theta) = \gamma_0\sqrt{1-(\varepsilon/2)\sin 2\theta}. \tag{18}$$

It reduces of course to the isotropic surface energy γ_0 of Eq. (16) in the $\varepsilon \to 0$ limit.

With the specific energies of Eqs. (15) and (17), the variational phase-field equations read

$$\begin{aligned} &\partial_j[\sigma_{ij}g(\phi)] = 0,\\ &\kappa[\nabla^2\phi + \varepsilon\partial_{xy}\phi] - g'(\phi)(\mathscr{E}_{strain} - \mathscr{E}_c) = \frac{1}{\chi}\partial_t\phi, \end{aligned} \tag{19}$$

where σ_{ij} is the usual stress tensor for an isotropic medium

$$\sigma_{ij} = \lambda u_{kk}\delta_{ij} + 2\mu u_{ij}. \tag{20}$$

Our aim in the following sections is to analyze the laws that govern the motion of a crack tip in this self-consistent description.

4. Laws of crack motion as solvability conditions

4.1. The tip inner problem

In the phase-field description, the obtention of laws of motion for a crack tip can be viewed as an "inner–outer" matching problem. The phase-field equation (19) introduce an intrinsic process zone scale $\xi = \sqrt{\kappa/(2\mathscr{E}_c)}$. The "inner" problem consists in the determination of a solution of Eq. (19) at the process zone scale ξ. The boundary conditions on this inner problem are imposed at a distance from the crack tip much greater than the process zone scale ($r \gg \xi$) and much smaller than any macroscopic length. They should coincide with the short-distance asymptotics of the "outer" problem, namely the usual determination of the elastic field for the crack under consideration. Therefore, the imposed boundary conditions on Eq. (19) are (i) that the material is intact ($\phi \to 1$) away from the crack itself and (ii) that for mixed mode I/II conditions, as considered in this section and the next one, the asymptotic behavior of the displacement field is

$$u_i(r,\Theta) \sim \frac{1}{4\mu}\sqrt{\frac{r}{2\pi}}[K_1\, d_i^{\mathrm{I}}(\Theta;v) + K_2\, d_i^{\mathrm{II}}(\Theta;v)], \tag{21}$$

where μ is the shear modulus and the functions d_i^m are directly related to the universal divergent forms of the stress (Eq. (1)) and are explicitly given (in polar coordinates) by Eqs. (C.6) and (C.7) of Appendix C. The values of K_1 and K_2 are imposed by the boundary conditions at the macroscopic scale and do not significantly vary when the crack tip advances by a distance of order ξ. In the frame of the crack tip moving at velocity v, Eqs. (19) thus read

$$\begin{aligned} &\partial_j[\sigma_{ij}g(\phi)] = 0,\\ &\kappa\nabla^2\phi - g'(\phi)(\mathscr{E}_{strain} - \mathscr{E}_c) = -\frac{v}{\chi}\partial_x\phi - \varepsilon\kappa\partial_{xy}\phi. \end{aligned} \tag{22}$$

4.2. Perturbative formalism and solvability conditions

Our first approach for obtaining the laws of crack tip motion consists in analyzing the slowly moving solutions of Eq. (22) with boundary conditions (21) perturbatively around an immobile Griffith crack. For isotropic elastic and phase-field energies and a pure opening mode, this Griffith crack corresponds to the stationary solution that exists for $\alpha(K_1^c)^2 = G_c$. Accordingly, we consider, for a small departure from Griffith threshold, $\delta K_1 = |K_1 - K_1^c|/K_1^c \ll 1$ and

[1] Note that with coordinates x', y' rotated by $\pi/4$ with respect to the x, y-axes, the phase-field energy reads, $\mathscr{E}_{pf} = (\kappa/2)(1+\varepsilon/2)(\partial_{x'}\phi)^2 + (\kappa/2)(1-\varepsilon/2)(\partial_{y'}\phi)^2$.

for a small $K_2 \ll K_1^c$, a slowly moving crack with a small (two-fold) anisotropy in ϕ-energy (Eq. (18)). Our aim is to find the relations between K_2 and the anisotropy, as well as between K_1, K_2 and the velocity v, required for the solution existence.

Linearization of Eqs. (22) around the isotropic Griffith crack $u_i^{(0)}, \phi^{(0)}$ with the substitutions $u_i = u_i^{(0)} + u_i^{(1)}, \phi = \phi^{(0)} + \phi^{(1)}$, gives

$$\begin{aligned} &\partial_j[\sigma_{ij}^{(1)} g(\phi^{(0)})] + \partial_j[\sigma_{ij}^{(0)} g'(\phi^{(0)})\phi^{(1)}] = 0, \\ &\kappa\nabla^2\phi^{(1)} - g'(\phi^{(0)})\sigma_{ij}^{(0)} u_{ij}^{(1)} - g''(\phi^{(0)})\phi^{(1)}[\mathscr{E}_{strain} - \mathscr{E}_c] = -\frac{v}{\chi}\partial_x\phi^{(0)} - \varepsilon\kappa\partial_{xy}\phi^{(0)}. \end{aligned} \tag{23}$$

This can symbolically be written as

$$\mathscr{L}\begin{pmatrix} u_1^{(1)} \\ u_2^{(1)} \\ \phi^{(1)} \end{pmatrix} = -\frac{v}{\chi}\begin{pmatrix} 0 \\ 0 \\ \partial_x\phi^{(0)} \end{pmatrix} - \varepsilon\kappa\begin{pmatrix} 0 \\ 0 \\ \partial_{xy}\phi^{(0)} \end{pmatrix}, \tag{24}$$

where $\mathscr{L}$ is the linear operator on the left-hand side (l.h.s.) of Eq. (23). The boundary conditions at infinity are that $\phi^{(1)}$ vanishes and that $u^{(1)}$ behaves asymptotically as in Eq. (21) but with K_1 replaced by δK_1, the small departure from Griffith threshold, and K_2 is also assumed to be small.

The linear operator $\mathscr{L}$ possesses two right zero-modes, that arise from the invariance of the zeroth-order problem under x and y translations, and can be explicitly obtained by infinitesimal translation of the immobile Griffith crack. For a general linear operator, the determination of the left zero-modes would nonetheless be a difficult problem. However, the variational character of the equations of motion imposes quite generally that $\mathscr{L}$ is self-adjoint (see Appendix B) and that left zero-modes are identical to right zero-modes. Thus, taking the scalar product of the two sides of Eq. (24) with the two translation zero-modes provides two explicit solvability conditions for Eq. (24).

The scalar product with a left zero-mode (u_1^L, u_2^L, ϕ^L) can generally be written as

$$\iint \mathrm{d}x\,\mathrm{d}y\,(u_1^L, u_2^L, \phi^L)\mathscr{L}\begin{pmatrix} u_1^{(1)} \\ u_2^{(1)} \\ \phi^{(1)} \end{pmatrix} = -\iint \mathrm{d}x\,\mathrm{d}y\ \phi^L\left\{\frac{v}{\chi}\partial_x\phi^{(0)} + \varepsilon\kappa\partial_{xy}\phi^{(0)}\right\}. \tag{25}$$

Since the left vector is a zero-mode of $\mathscr{L}$, the only contribution to the l.h.s. of Eq. (25) comes from boundary terms,

$$\begin{aligned} \iint \mathrm{d}x\,\mathrm{d}y\,(u_1^L, u_2^L, \phi^L)\mathscr{L}\begin{pmatrix} u_1^{(1)} \\ u_2^{(1)} \\ \phi^{(1)} \end{pmatrix} = \oint \mathrm{d}s\, n_j\{&[u_i^L\sigma_{ij}^{(1)} - u_i^{(1)}\sigma_{ij}^L]\, g(\phi^{(0)}) \\ &+ [u_i^L\phi^{(1)} - u_i^{(1)}\phi^L]g'(\phi^{(0)})\sigma_{ij}^{(0)} + \kappa[\phi^L\partial_i\phi^{(1)} - \phi^{(1)}\partial_i\phi^L]\}, \end{aligned} \tag{26}$$

where $\mathbf{n}$ is the outward contour normal and the contour integral is taken counterclockwise along a circle (of radius r) centered on the fracture tip.

4.3. Translations along x and crack velocity

The zero-mode corresponding to translations along x is $(\partial_x u_1^{(0)}, \partial_x u_2^{(0)}, \partial_x\phi^{(0)})$. On the r.h.s. of Eq. (25), the term proportional to the anisotropy ε vanishes (by symmetry or explicit integration). The r.h.s. of Eq. (26) can be simplified since on a circle of a large enough radius, $g(\phi^{(0)})$ equals unity everywhere except in the region where the circle cuts the fracture lips. This region of non-constant ϕ is far away from the crack tip where the crack is to a very good approximation invariant by translation along x and $\partial_x\phi \simeq \partial_x\mathbf{u} \simeq 0$. Therefore,

$$\begin{aligned} \iint \mathrm{d}x\,\mathrm{d}y(\partial_x u_1^{(0)}, \partial_x u_2^{(0)}, \partial_x\phi^{(0)})\mathscr{L}\begin{pmatrix} u_1^{(1)} \\ u_2^{(1)} \\ \phi^{(1)} \end{pmatrix} &= \oint \mathrm{d}s\, n_i[u_i^{(x;I)}\sigma_{ij}^{(1)} - u_i^{(1)}\sigma_{ij}^{(x;I)}] \\ &= -\frac{K_1\delta K_1}{\mu}(1-v), \end{aligned} \tag{27}$$

where the explicit formulas (C.6), (C.7) for the elastic displacements around a straight crack, have been used to obtain the last equality as detailed in Appendix C (see Eq. (C.14)). Comparison between Eqs. (27) and (25) finally provides the natural

result that the crack velocity is proportional to the departure from Griffith threshold,

$$\frac{v}{\chi}\iint \mathrm{d}x\,\mathrm{d}y[\partial_x\phi^{(0)}]^2 = \frac{K_1\,\delta K_1}{\mu}(1-\nu) = \delta G. \tag{28}$$

4.4. Translations along y and crack direction

A second condition on crack motion arises from the zero-mode corresponding to translations along y, $(\partial_y u_1^{(0)}, \partial_y u_2^{(0)}, \partial_y \phi^{(0)})$. In this case, only the term proportional to the anisotropy ε contributes to the l.h.s. of Eq. (26).

$$\iint \mathrm{d}x\,\mathrm{d}y\,\partial_y\phi^{(0))}\partial_{xy}\phi^{(0))} = -\frac{1}{2}\int \mathrm{d}y[\partial_y\phi^{(0))}|_{x=-\infty}]^2. \tag{29}$$

Similarly to Eq. (27), the r.h.s. of Eq. (26) simplifies when the integration contour is a large enough circle

$$\begin{aligned}\iint \mathrm{d}x\,\mathrm{d}y(\partial_y u_1^{(0)}, \partial_y u_2^{(0)}, \partial_y\phi^{(0)})\mathscr{L}\begin{pmatrix} u_1^{(1)} \\ u_2^{(1)} \\ \phi^{(1)}\end{pmatrix} &= \oint \mathrm{d}s\, n_i[u_i^{(y;I)}\sigma_{ij}^{(1)} - u_i^{(1)}\sigma_{ij}^{(y;I)}] \\ &= \frac{K_1 K_2}{\mu}(1-\nu),\end{aligned} \tag{30}$$

where again the explicit evaluation in the last equality is detailed in Appendix C (see Eq. (C.20)). Thus, the second relation of crack motion reads

$$\frac{K_1 K_2}{\mu}(1-\nu) = \frac{\varepsilon\kappa}{2}\int_{-\infty}^{+\infty} \mathrm{d}y[\partial_y\phi^{(0))}|_{x=-\infty}]^2. \tag{31}$$

Eq. (31) reduces to the principle of local symmetry (i.e. $K_2 = 0$) for an isotropic medium and provides the appropriate generalization for the considered anisotropy. Before further discussing these results and their physical consequences, we present a different derivation in the next section.

5. Generalized Eshelby–Rice integrals

The second approach, which we pursue here, directly exploits the variational character of the equations of motion and their invariance under translation. It yields identical solvability conditions as the approach of Section 4 when $G - G_c$ and symmetry breaking perturbations are small, but it is more general since it does not require these quantities to be small.

5.1. The generalized Eshelby tensor

As shown by Noether (1918) in her classic work, to each continuous symmetry of variational equations is associated a conserved quantity (charge) and an allied divergenceless current. Space (and time) translation invariance are well known to give the divergenceless energy–momentum tensor in field theories (Landau and Lifshitz, 1975). Eshelby (1951) and following authors (Rice, 1968; Eshelby, 1975; Gurtin and Podio-Guidugli, 1998; Adda-Bedia et al., 1999; Oleaga, 2001) have shown the usefulness of the analogous tensor for classical elasticity theory. Here, we consider the generalized energy–momentum (GEM) tensor which extends the Eshelby (1975) tensor for linear elastic fields by incorporating short-scale physics through its additional dependence on the phase-field ϕ.

We find it convenient to define the four-dimensional vector field $\psi^\alpha = u_\alpha$ for $1 \leqslant \alpha \leqslant 3$ and $\psi^\alpha = \phi$ for $\alpha = 4$, where u_α are the components of the standard displacement field. The inner problem Eq. (22) can then be rewritten in the condensed form

$$-\delta_{\alpha,4}\,v\,\chi^{-1}\partial_1\phi = \partial_j\frac{\partial\mathscr{E}}{\partial[\partial_j\psi^\alpha]} - \frac{\partial\mathscr{E}}{\partial\psi^\alpha}, \quad \alpha = 1,\ldots,4, \tag{32}$$

where here and in the following summation is implied on repeated indices (from 1 to 3 on roman indices and from 1 to 4 on greek ones). Chain rule differentiation provides the simple equality,

$$\partial_i\mathscr{E} = \frac{\partial\mathscr{E}}{\partial\psi^\alpha}\partial_i\psi^\alpha + \frac{\partial\mathscr{E}}{\partial[\partial_j\psi^\alpha]}\partial_j\partial_i\psi^\alpha. \tag{33}$$

Using Eq. (32) to eliminate $\partial\mathscr{E}/\partial\psi_\alpha$ from the r.h.s. of Eq. (33), we obtain

$$\partial_j T_{ij} = \frac{v}{\chi}\partial_1\phi\partial_i\phi \quad \text{for } i = 1,2, \tag{34}$$

where the GEM tensor T_{ij} reads

$$T_{ij} \equiv \mathscr{E}\delta_{ij} - \frac{\partial \mathscr{E}}{\partial[\partial_j \psi^\alpha]}\partial_i \psi^\alpha. \tag{35}$$

The GEM tensor T_{ij} is the sought extension of the classical Eshelby (1951) tensor T^E_{ij} of classical linear elasticity

$$T^E_{ij} = \mathscr{E}_{strain}\delta_{ij} - \sigma_{jk}\partial_i u_k. \tag{36}$$

The GEM tensor T_{ij} reduces identically to T^E_{ij} in the intact material where the phase-field is constant ($\phi = 1$). Both tensors are non-symmetric in their two indices. The divergence of the GEM tensor taken on its second indice vanishes in the zero-velocity limit, when dissipation in the process zone also vanishes.

5.2. Laws of crack motion

In order to take advantage of Eq. (34), we integrate the divergence of the GEM tensor over a large disk Ω centered on the crack tip (see Fig. 2), following Eshelby (1975) computation of the configurational force on the crack tip treated as a defect in a linear elastic field and subsequent attempts to derive criteria for crack propagation and stability (Gurtin and Podio-Guidugli, 1998; Adda-Bedia et al., 1999; Oleaga, 2001). The important difference with these previous computations is that, here, the GEM tensor (35) is well defined everywhere, so that the crack itself is included in the domain of integration. The integral of the divergence of the GEM tensor can be written as a contour integral over the large circle $\partial\Omega$ bounding the disk Ω,

$$F_i = \int_{C_{A\to B}} \mathrm{d}s\, T_{ij}\, n_j + \int_{B\to A} \mathrm{d}s\, T_{ij} n_j - \frac{\nu}{\chi}\int_\Omega d\vec{x}\,\partial_1\phi\partial_i\phi = 0. \tag{37}$$

We have decomposed the circle $\partial\Omega$ into: (i) a large loop $C_{A\to B}$ around the tip in the unbroken material, where A (B) is at a height h below (above) the crack axis that is much larger than the process zone size but much smaller than the radius R of the contour, $\xi \ll h \ll R$ and (ii) the segment ($B \to A$) that traverses the crack from B to A behind the tip, as illustrated in Fig. 2. In both integrals, ds is the contour arclength element and n_j the components of its outward normal.

Eq. (37) provides an alternative basis to predict the crack speed and its path for quasistatic fracture. The F_i's can be interpreted as the parallel ($i = 1$) and perpendicular ($i = 2$) components with respect to the crack direction, of the sum of all forces acting on the crack tip. In Eq. (37), the three integrals terms from left to right, respectively, represent configurational, cohesive, and dissipative forces. We examine them in turn.

5.2.1. Configurational forces and Eshelby torque

We take A and B far back from the tip and close to the crack on a macroscopic scale but with the distance $2h$ between A and B much larger than the process zone scale. Namely, we consider the mathematical limit $h \to +\infty$, $R \to +\infty$ with $h/R \to 0$ where R is the distance from A and B to the crack tip. In this limit, the first integral in Eq. (37) is taken on a path that is entirely in the unbroken material where ϕ is constant and equal to unity. Thus, the tensor T_{ij} reduces to the classical Eshelby tensor T^E_{ij} (Eq. (36)) the first integral in Eq. (37) yields the two components of the usual configurational forces $F^{(conf)}_i$,

$$F^{(conf)}_i = \int_{C_{A\to B}} \mathrm{d}s\, T^E_{ij}\, n_j. \tag{38}$$

The first component, $F^{(conf)}_1$, is the crack extension force and also Rice's (1968) J integral,

$$F^{(conf)}_1 = \int_{C_{A\to B}} \mathrm{d}s\, T^E_{1j}\, n_j. \tag{39}$$

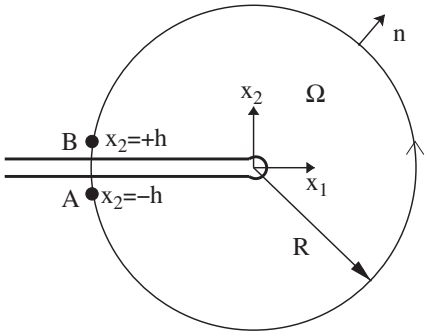

Fig. 2. Spatially diffuse crack tip region with $\phi = \frac{1}{2}$ contour separating broken and unbroken material (thick solid line).

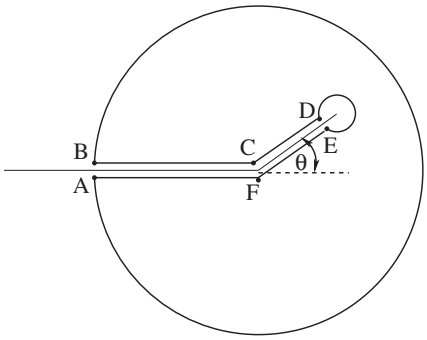

Fig. 3. Sketch showing the contour integral decomposition in Eq. (42). The crack with its virtual extension at an angle θ is depicted by the thick bold line. The integral contour follows the great circle from A to B; it continues along the upper lip of the crack from B to C and then along the upper lip of the virtual extension from C to D; it then encircles the extended crack tip following the small circle from D to E; finally it comes back to A along the lower crack lips via F.

With the known forms of the elastic displacement fields near the crack tip, as detailed in Appendix C (see Eq. (C.28)), one obtains the well-known expression (2) of the crack extension force,

$$F_1^{(conf)} = G = \alpha(K_1^2 + K_2^2). \tag{40}$$

The second component $F_2^{(conf)}$ can be computed in an analogous way from the elastic displacement fields near the crack tip, (Eq. (C.29)) and one obtains

$$F_2^{(conf)} = -2\alpha K_1 K_2. \tag{41}$$

As discussed earlier, $F_2^{(conf)}$ is the Eshelby (1975) torque that can be interpreted physically if one imagine extending the crack tip by a small amount at a small angle θ from the main tip axis. Then $F_2^{(conf)}$ is equal to the angular derivative of the crack extension force $G(\theta)$ at $\theta = 0$.

This equality can be seen in two ways. First, we can use the general properties of the Eshelby tensor. We denote with a tilde the elastic quantities corresponding to the crack with the small extension of length s at an angle θ. Since the crack extension is along the direction $(\cos(\theta), \sin(\theta))$, we consider the allied vector obtained from the Eshelby tensor, $\tilde{T}^E_{\theta j} \equiv \cos(\theta)\tilde{T}^E_{1j} + \sin(\theta)\tilde{T}^E_{2j}$. The flux of this vector vanishes when taken through the contour that goes along the great circle from A to B and then continues in a classical way along the lips of the extended crack, as drawn in Fig. 3.

$$\left(\int_{C_{A\to B}} + \int_{B\to C} + \int_{C\to D} + \int_{C_{D\to E}} + \int_{E\to F} + \int_{F\to A}\right) \mathrm{d}s\, \tilde{T}^E_{\theta j}\, n_j = 0. \tag{42}$$

The two integrals on the fracture lips from C to D and E to F do not contribute since the integrand vanishes: the θ direction is along the path and the normal stresses vanish on the fracture lips. The same argument shows that the integrand is simply equal to $\pm\tilde{\mathscr{E}}_{strain}\sin(\theta)$ for the integrals from B to C and F to A along the lips of the original fracture. The integral on the small circle around the extended crack tip $C_{D\to E}$ is equal to $-\tilde{G}(\theta)$ where $\tilde{G}(\theta)$ is the energy-release-rate at the end of the small crack extension. Eq. (42) thus reduces to

$$\int_{C_{A\to B}} [\cos(\theta)\tilde{T}^E_{1j} + \sin(\theta)\tilde{T}^E_{2j}]\, n_j = \tilde{G}(\theta) + \int_R^0 \mathrm{d}x \sin(\theta)[\tilde{\mathscr{E}}^+_{strain}(x) - \tilde{\mathscr{E}}^-_{strain}(x)], \tag{43}$$

where $\tilde{\mathscr{E}}^+_{strain}$ and $\tilde{\mathscr{E}}^-_{strain}$, respectively, denote the elastic strain energy densities on the upper and lower fracture lips. The required identity between $F_2^{(conf)}$ and the angular derivative of $\mathrm{d}\tilde{G}/\mathrm{d}\theta|_{\theta=0}$ follows from differentiation of Eq. (43) with respect to θ at $\theta = 0$. When this is performed, there are two kinds of terms. Terms coming from the differentiation of the explicit trigonometric functions in Eq. (43) and terms coming from the implicit dependence upon θ of tilde quantities. However, in the integral on the l.h.s of Eq. (43), these implicit terms vanish as the length s of the extension is taken to zero, and in the integral on the r.h.s. they are multiplied by a vanishing sine function. Moreover, for the straight fracture at $\theta = 0$, only σ_{xx} is non-zero on the fracture lips and it is of opposite sign on the upper and lower fracture lips (Eq. (C.4)). The strain energy densities which are quadratic in the stress σ_{xx} are therefore equal on the upper and lower fracture lips and after differentiation, the contribution of integral term on the r.h.s. of Eq. (43) vanishes at zero.[2] Finally, in the limit of a vanishing extension length ($s \to 0$) tilde quantity tend toward their (non-tilde) values on the original fracture and one obtains

$$F_2^{(conf)} = \int_{C_{A\to B}} T^E_{2j} n_j = \lim_{s\to 0} \frac{\mathrm{d}\tilde{G}(\theta)}{\mathrm{d}\theta}\bigg|_{\theta=0} \equiv G_\theta(0). \tag{44}$$

[2] Subdominant terms, coming for instance from a macroscopic curvature of the crack, could be different on the two crack lips but note that the integral range is on a length scale that is vanishingly small on a macroscopic scale.

This relation between the second component $F_2^{(conf)}$ and the angular derivative of $G(\theta)$ can also be obtained by comparing their explicit expressions in term of the SIF K_1 and K_2. As it is well known, the SIF $\tilde{K}_1$ and $\tilde{K}_2$ at the end of a small extension can be expressed as linear combination of K_1 and K_2 (Amestoy and Leblond, 1992)

$$\tilde{K}_1 = F_{11}(\theta)K_1 + F_{12}(\theta)K_2,$$
$$\tilde{K}_2 = F_{21}(\theta)K_1 + F_{22}(\theta)K_2, \tag{45}$$

with clearly $F_{11}(0) = F_{22}(0) = 1$ and $F_{12}(0) = F_{21}(0) = 0$ and the derivative at $\theta = 0$, $F'_{11}(0) = F'_{22}(\theta) = 0$, as already mentioned in Section 2 (Eqs. (6) and (7)). A detailed computation (Amestoy and Leblond, 1992) provides the other two derivatives $F'_{12}(0) = -\frac{3}{2}$ and $F'_{21}(0) = \frac{1}{2}$. Therefore, one obtains

$$\lim_{s\to 0} \frac{\mathrm{d}\tilde{G}(\theta)}{\mathrm{d}\theta}\bigg|_{\theta=0} = 2\alpha K_1 K_2 [F'_{12}(0) + F'_{21}(0)] = -2\alpha K_1 K_2. \tag{46}$$

This is indeed identical to the expression of $F_2^{(conf)}$ obtained by a direct computation (Eq. (41)) and it provides a second derivation of Eq. (44).

5.2.2. Cohesive forces

An important new ingredient in Eq. (37) is the second portion of the line integral ($\int_{B\to A}$) of the GEM tensor that traverses the crack. This integral represents physically the contributions of cohesive forces inside the process zone. To see this, we first note that the profiles of the phase field and the three components of the displacement can be made to depend only on x_2 provided that the contour is chosen much larger than the process zone size and to traverse the crack perpendicularly from B to A. With this choice, we have that $n_1 = -1$, $n_2 = 0$, along this contour and therefore that, for $i = 1$

$$F_1^{(coh)} = \int_{B\to A} \mathrm{d}s\, T_{1j} n_j = -\int_{-h}^{+h} \mathrm{d}x_2\, T_{11}. \tag{47}$$

The spatial gradients parallel to the crack direction ($\partial_1 \psi^k$) give vanishingly small contributions in the limit $h/\xi \to +\infty$ and $R/\xi \to +\infty$ with $h/R \to 0$. Thus, the integrand on the r.h.s. of Eq. (47) reduces to the energy of a one-dimensional crack which, as recalled in Appendix A (Eq. (A.22)), is itself independent of the strain and can be identified to twice the surface energy γ

$$F_1^{(coh)} = -\int_{-h}^{+h} \mathrm{d}x_2\, \mathscr{E}(\phi, \partial_2\phi, \partial_2 u_2) = -2\gamma. \tag{48}$$

This yields the expected result that cohesive forces along the crack direction exert a force opposite to the crack extension force with a magnitude equal to twice the surface energy.

One similarly obtains for $i = 2$, in the same limit $\xi \ll h \ll R$, the other component $F_2^{(coh)}$ of the force perpendicular to the crack direction

$$F_2^{(coh)} = \int_{B\to A} \mathrm{d}s\, T_{2j} n_j = -\int_{-h}^{+h} \mathrm{d}x_2\, T_{21} = \int_{-h}^{+h} \mathrm{d}x_2 \frac{\partial \mathscr{E}}{\partial \partial_1 \psi_\alpha} \partial_2 \psi_\alpha = \int_{-h}^{+h} \mathrm{d}x_2 \frac{\partial \mathscr{E}_{pf}}{\partial \partial_1 \phi} \partial_2 \phi. \tag{49}$$

The last equality comes from the fact that the only considered anisotropy is in the phase-field part $\mathscr{E}_{pf}$ of the energy density and that, as above, gradients parallel to the crack direction give negligible contributions far behind the crack tip. $F_2^{(coh)}$ can be expressed as the angular derivative of the surface energy at the crack tip direction $\theta = 0$. For a material broken along a line lying at a direction θ with the x-axis, the displacement and phase fields only depend on the normal coordinate $\eta = -x_1 \sin(\theta) + x_2 \cos(\theta)$. The local energy density $\mathscr{E}[\phi, \partial_1\phi, \partial_2\phi, \partial_\eta u_\eta]$ is therefore equal to $\mathscr{E}[\phi, -\sin(\theta)\partial_\eta\phi, \cos(\theta)\partial_\eta\phi, \partial_\eta u_\eta]$. The allied surface energy reads

$$2\gamma(\theta) = \int_{-\infty}^{+\infty} \mathrm{d}\eta\ \mathscr{E}[-\sin(\theta)\partial_\eta\phi, \cos(\theta)\partial_\eta\phi, \partial_\eta u_\eta]. \tag{50}$$

Differentiation with respect to θ brings on the r.h.s. of Eq. (50) terms coming from the explicit dependence of the integrand on θ as well as terms coming from the implicit dependence of the fields on the breaking angle (for an anisotropic material). However, the contribution of the implicit terms vanishes since for any given angle the fields minimize the total energy and no field variation leads to an energy change at linear order. Therefore, one obtains

$$2\frac{\mathrm{d}}{\mathrm{d}\theta}\gamma\bigg|_{\theta=0} = \int_{-\infty}^{+\infty} \mathrm{d}x_2 \frac{\partial \mathscr{E}}{\partial \partial_1 \phi}(-\partial_2\phi) = \int_{-\infty}^{+\infty} \mathrm{d}x_2 \frac{\partial \mathscr{E}_{pf}}{\partial \partial_1 \phi}(-\partial_2\phi), \tag{51}$$

since η reduces to x_2 for $\theta = 0$. Comparison of Eqs. (49) and (51) shows that

$$F_2^{(coh)} = -2\frac{\mathrm{d}}{\mathrm{d}\theta}\gamma\bigg|_{\theta=0} \tag{52}$$

as announced.

Of course, relation (52) can also be checked by direct computation for any explicit form of the phase-field energy. For instance, in the simple case of Eq. (17), one obtains from Eq. (49),

$$F_2^{(coh)} = \int \mathrm{d}x_2 \frac{\partial \mathscr{E}_{pf}}{\partial \partial_1 \phi} \partial_2 \phi = \frac{\varepsilon}{2} \int \mathrm{d}x_2 \, \kappa (\partial_2 \phi)^2 = \varepsilon \gamma_0, \tag{53}$$

where, for the last equality, it should be noted (see Appendix A) that the second integral in Eq. (53) is equal to the energy (by unit length) of the cracked material which is itself equal to $2\gamma_0$. The result of Eq. (53) indeed agrees with Eq. (52), $\varepsilon\gamma_0 = -2\gamma_\theta(0)$, since the surface energy in the direction θ is given by Eq. (18).

The force $F_2^{(coh)}$ is the direct analog of the Herring (1951, p. 143) torque $\gamma_\theta = \mathrm{d}\gamma/\mathrm{d}\theta$ on grain boundaries. This torque tends to turn the crack into a direction that minimizes the surface energy.

5.2.3. Dissipative forces

The last term in Eq. (37) gives the two components of the dissipative force

$$F_i^{(dis)} = v\chi^{-1} \int_{-\infty}^{+\infty} \int_{-\infty}^{+\infty} \mathrm{d}x_1 \, \mathrm{d}x_2 \, \partial_1 \phi \partial_i \phi. \tag{54}$$

The limit where the disk area Ω tends to infinity has been taken since the integrand vanishes outside the process zone. In contrast to the configurational and cohesive forces, the dissipative force clearly depends on the detail of the underlying diffuse interface model.

5.2.4. Force-balance and anisotropic generalization of the principle of local symmetry

Substituting the results of Eqs. (39)–(54) into Eq. (37), the two conditions of Eq. (37) can be rewritten in the compact form

$$F_1 = G - G_c - F_1^{(dis)} = 0, \tag{55}$$

$$F_2 = G_\theta(0) - G_{c\theta}(0) - F_2^{(dis)} = 0, \tag{56}$$

where we have used the fact that $G_{c\theta} = 2\gamma_\theta$. Eq. (55) together with Eq. (54) predicts the crack speed for G close to G_c

$$v \approx \frac{\chi}{\iint \mathrm{d}x_1 \, \mathrm{d}x_2 (\partial_1 \phi_0)^2} (G - G_c), \tag{57}$$

where ϕ_0 is the phase-field profile for a stationary crack (Karma and Lobkovsky, 2004), and thus the integral in the denominator above is just a constant of order unity. Eq. (56), in turn, predicts the crack path by imposing K_2 at the crack tip,

$$K_2 = -(G_{c\theta}(0) + F_2^{(dis)})/(2\alpha K_1). \tag{58}$$

The component $F_2^{(dis)}$ of the dissipative force vanishes with the crack velocity in the quasistatic limit. So, in this limit, the microscopic details of the process zone do not play a role and the crack direction is uniquely determined by the directional anisotropy of the material through the simplified condition

$$K_2 = -G_{c\theta}(0)/(2\alpha K_1). \tag{59}$$

Eq. (59) replaces the principle of local symmetry for a material with an anisotropic surface tension energy. It reduces of course to the principle of local symmetry in an isotropic material, since then $G_{c\theta}$ vanishes. One can also note that quite remarkably, Eq. (59) only contains macroscopically defined parameters and is independent of the detailed physics of the process zone.

Outside the quasistatic limit, $K_2 = 0$ should continue to hold for an isotropic material since $F_2^{(dis)}$ vanishes even for a finite crack speed. The latter follows from the symmetry of the inner phase-field solution for a propagating crack with $K_2 = 0$, $\phi(x_1, x_2) = \phi(x_1, -x_2)$, which implies that the product $\partial_1\phi\partial_2\phi$ in Eq. (54) is anti-symmetric and that the spatial integral of this product vanishes. In an anisotropic material, however, ϕ is generally not symmetrical about the local crack axis and $F_2^{(dis)}$ should generally be non-zero. The crack direction should then become dependent on the details of the energy dissipation in the process zone.

A small velocity expression for the dissipative force perpendicular to the crack axis can be obtained by considering the phase-field profile that corresponds to a stationary Griffith crack in an anisotropic material. Here, ϕ_0^A, is uniquely defined as the stationary phase-field profile that exists for a unique pair of values of K_1 and K_2 that satisfy the conditions of equilibrium parallel and perpendicular to the crack axis, $\alpha(K_1^2 + K_2^2) = G_c(0)$ and $-2\alpha K_1 K_2 = G_{c\theta}(0)$, respectively. For small velocity, Eq. (54) must therefore reduce to $F_2^{(dis)} = v\chi^{-1} I(0)$ where the integral

$$I(0) \equiv \int \mathrm{d}x_1 \, \mathrm{d}x_2 \, \partial_1 \phi_0^A \partial_2 \phi_0^A \tag{60}$$

is a dimensionless constant that, like G_c and $G_{c\theta}$, depends generally on the local orientation of the crack with respect to some fixed reference axis chosen here as $\theta = 0$. For small velocity, Eq. (58) therefore becomes

$$K_2 = -(G_{c\theta}(0) + v\chi^{-1}I(0))/(2\alpha K_1), \tag{61}$$

where $I(0)$ vanishes in the isotropic limit since ϕ_0^A approaches ϕ_0 and hence becomes symmetrical about the crack axis in that limit.

5.3. Comparison with the maximum energy-release-rate criterion

In isotropic materials, the principle of local symmetry and the maximum-energy-release-rate criterion coincide for smooth cracks but give slightly different results in general. A well-studied case is the growth of a kink extension at the tip of a straight crack, as discussed below.

For smooth cracks, it should be noted that force-balance, the present anisotropic generalization (Eq. (59)) of the principle of local symmetry, also coincides with a generalization of the maximum energy-release-rate criterion to anisotropic materials. One way to define the latter is to require crack growth to take place in the direction that maximizes $\tilde{G}(\theta) - 2\gamma(\theta)$ (Leblond, 2005) where as before $\tilde{G}(\theta)$ is the energy-release-rate for an infinitesimal extension at the crack tip at an angle θ (and $\theta = 0$ is the direction of the unextended crack). For a smooth crack, the condition that this quantity be maximal in the crack direction yields

$$\frac{\mathrm{d}}{\mathrm{d}\theta}[\tilde{G}(\theta) - 2\gamma(\theta)]_{\theta=0} = 0. \tag{62}$$

With the help of Eq. (46), this is seen to be identical to Eq. (59) as stated.

For non-smooth crack paths, force-balance (Eq. (59)) and the maximum energy-release-rate criterion give different predictions. The growth of a kinked extension at the tip of a straight crack subject to mixed-mode I/II loading has been studied as a test case by many authors (see e.g. Amestoy and Leblond, 1992; Hutchinson and Suo, 1992) and references therein). Although distinct, the predictions for the threshold energy-release-rates and the kink angles in an isotropic medium are very close for the two criteria. Thus for isotropic media, the difference between the two criteria is insignificant in practice but nonetheless leads to some questions of theoretical interest.[3] For instance, it has remained unclear what the fate of a crack would be if loaded in the narrow gap in which kink propagation is allowed by the maximum energy-release-rate criterion but forbidden by the principle of local symmetry.

Interestingly, the situation is different for a kinked crack in an anisotropic medium. It is not difficult to find cases where there is a significant difference between the kink angles predicted by the maximum energy-release-rate criterion and the force-balance condition (Eq. (59)) which generalizes the principle of local symmetry. As a simple illustration, we consider the growth of a straight crack with a load creating a mixed-mode singular stress distribution at the crack tip, with SIF K_1 and K_2 (Eq. (1)). The SIFs $\tilde{K_1}(\theta)$ and $\tilde{K_2}(\theta)$ at the end of a small extension, at an angle θ with the direction of the main crack, are given as linear combinations of K_1 and K_2 as described by Eq. (45). With these notations, the energy-release-rate at the tip of the small extension reads

$$\tilde{G}(\theta) = \alpha[\tilde{K_1}(\theta)^2 + \tilde{K_2}(\theta)^2]. \tag{63}$$

Force-balance, Eq. (59), predicts that above the Griffith threshold G_{fb}, a kinked extension will grow at an angle θ_{fb} such that

$$G_{fb} = \tilde{G}(\theta_{fb}) = 2\gamma(\theta_{fb}), \tag{64}$$

$$-2\alpha\tilde{K_1}(\theta_{fb})\tilde{K_2}(\theta_{fb}) - 2\left.\frac{\mathrm{d}\gamma}{\mathrm{d}\theta}\right|_{\theta=\theta_{fb}} = 0. \tag{65}$$

Maximum energy- release-rate predicts the different Griffith threshold G_{mer} and extension angle θ_{mer} that satisfy

$$G_{mer} = G(\theta_{mer}) = 2\gamma(\theta_{mer}), \tag{66}$$

$$\left.\frac{\mathrm{d}\tilde{G}}{\mathrm{d}\theta}\right|_{\theta=\theta_{mer}} - 2\left.\frac{\mathrm{d}\gamma}{\mathrm{d}\theta}\right|_{\theta=\theta_{mer}} = 0. \tag{67}$$

We have numerically investigated the difference between these two predictions for a simple two-fold anisotropy

$$\gamma(\theta) = \gamma_0\sqrt{1 - \tfrac{1}{2}\cos(2\theta)}, \tag{68}$$

where, for convenience, the anisotropy axes have been rotated by $\pi/4$ compared to our previous choice (Eq. (18)) and we have purposely chosen a large value of $\varepsilon = 1$ to produce an example where the kink angles predicted by the principle of maximum energy-release-rate and the force-balance condition differ markedly. As before, the direction of the main crack stands at $\theta = 0$.

[3] We are indebted to J.J. Marigo for emphasizing this point to us.

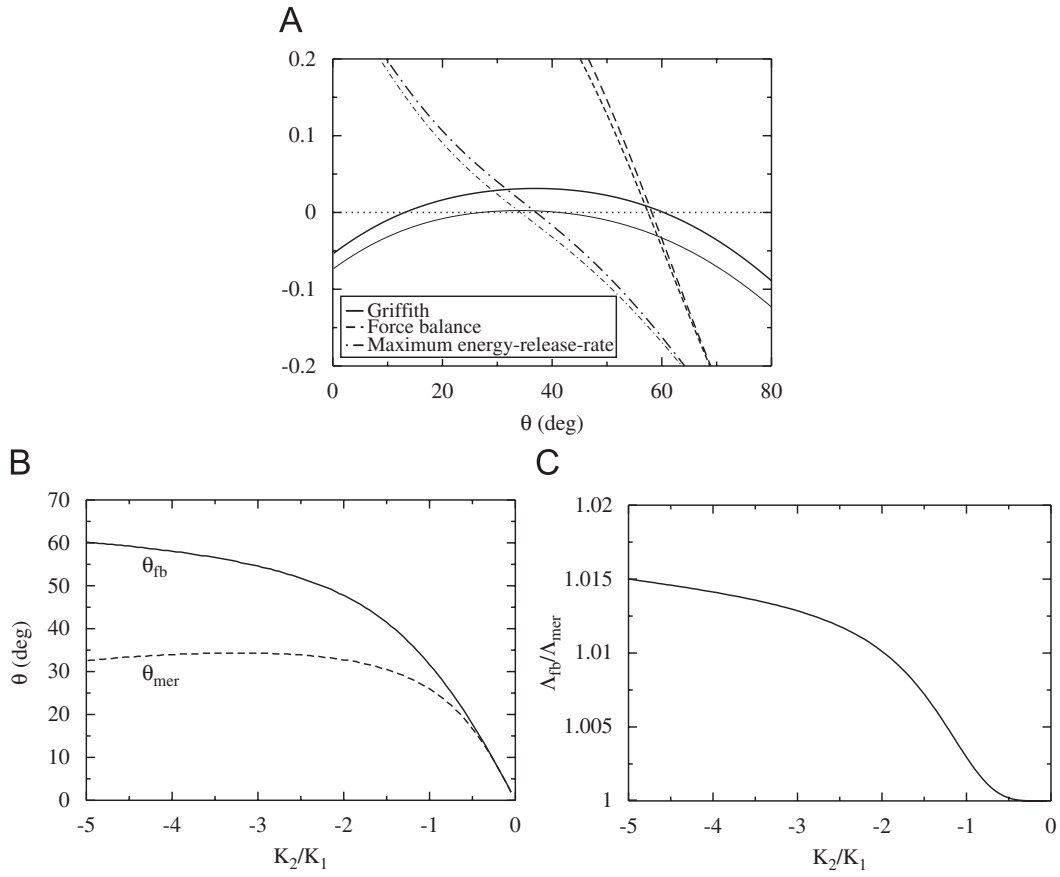

Fig. 4. Comparison of force-balance and maximum energy-release-rate criterion predictions for a kink growing at the tip of a main crack under mixed-mode loading in an infinite medium with anisotropic surface energy given by Eq. (68). (A) The angles predicted by the two criteria are shown for the particular SIF ratio $K_1/K_2 = -4$ and two different loads, one (thin lines) just above the threshold load for the maximum energy-release-rate and the other (thick lines) just above the threshold load for the force-balance criterion. For the maximum energy-release-rate threshold load, the adimensioned difference between the energy-release-rate at the small extension tip and the anisotropic interface energy $[\tilde{G}(\theta) - 2\gamma(\theta)]/(2\gamma_0)$ (thin solid line) is negative everywhere except near the maximum $\theta_{mer} \simeq 34^\circ$. The derivative of this curve (thin dot-dashed line) intersects zero at θ_{mer}, the angle predicted by the maximum energy-release-rate criterion (Eq. (67)). The angle θ_{fb} predicted by force-balance, $\theta_{fb} \simeq 57.5^\circ$, is given by the vanishing of the force-balance condition (thin dashed line, Eq. (65) plotted here in an adimensioned form after division by $2\gamma_0$) but it does not correspond to a growing extension since $[\tilde{G}(\theta_{fb}) - 2\gamma(\theta_{fb})]/(2\gamma_0)$ is negative for this load. The thick lines show analogous curves for the slightly larger load that corresponds to the threshold of propagation for the force-balance condition. The intersection of the force-balance condition (thick dashed line) with zero gives $\theta_{fb} \simeq 58^\circ$ at threshold. (B) Kink angle as a function of K_1/K_2 for force-balance (θ_{fb}, solid line) and maximum energy-release-rate (θ_{mer} dashed line) at the Griffith threshold for crack growth at that particular angle. (C) ratio of the threshold loads for growth predicted by the two criteria as measured by the ratio $\Lambda_{fb}/\Lambda_{mer}$ of the threshold SIFs for the parent crack (see main text for details).

The computation of the energy-release-rate at the tip of the small extension $\tilde{G}(\theta)$ and of its derivative requires the evaluation of the functions $F_{ij}(\theta)$ (Eq. (45)) and of their derivatives for finite angles. This has been performed by using the series expansions of the F_{ij}'s (up to order θ^{20}) as given by Amestoy and Leblond (1992).[4] We imagine that the load on the parent crack as measured by the SIFs at its tip is given by $K_1 = \Lambda(2\gamma_0/\alpha)^{1/2}$, $K_2 = \Lambda\rho_k(2\gamma_0/\alpha)^{1/2}$, where the factor $(2\gamma_0/\alpha)^{1/2}$ is introduced for convenience to make Λ dimensionless ($\Lambda = 2^{-1/4}$ corresponds to the onset of propagation of a straight crack for $\rho_K = 0$ for the anisotropy (68)). As shown in Fig. 4A, when Λ is increased from zero, keeping a *constant ratio* $\rho_K = K_1/K_2$ of the mode I and II SIFs, a first critical value Λ_{mer} is attained for which the maximum energy-release-rate criterion allows kink growth at angle θ_{mer}. When Λ is increased further a second critical value, Λ_{fb}, is reached for which the kinked extension can grow at an angle θ_{fb} with force-balance holding at its tip. The obtained values of the extension angles and of the ratio $\Lambda_{fb}/\Lambda_{mer}$ are displayed in Fig. 4B and C, as a function of the ratio $\rho_K = K_2/K_1$.

As in the isotropic case, the load difference between the two criteria remains small (of the order of 1% in the present case, as seen in Fig. 4C) but, quite remarkably, it is seen in Fig. 4B that the presence of anisotropy (Eq. (68)) renders the angle difference between the two criteria much more pronounced than in an isotropic medium. The large angle difference opens up the possibility to discriminate between the two criteria in full numerical simulations. Also, even though the "forbidden" gap between the threshold loads for propagation given by the maximum energy-release-rate and

[4] We have checked that these series give a very precise estimation of the $F_{ij}(\theta)$'s up to $\theta = 90^\circ$, by comparison with the full numerical evaluations of Katzav et al. (2007).

force-balance conditions is small, it is interesting to inquire what happens for loads inside this gap in simulations. These questions are explored in Section 7.

5.4. Crystalline materials

Our results have interesting implications for crack propagation in crystalline materials. Basic experimental studies have demonstrated the existence of both "cleavage cracks", which are cracks that propagate along low energy crystal planes, such as {1 1 1} (Hauch et al., 1999) or {1 1 0} (Deegan et al., 2003) in silicon, and smooth cracks (Deegan et al., 2003) that resemble qualitatively the cracks seen in isotropic materials. While the propensity for crack propagation along cleavage planes in crystalline materials is to be expected energetically, the observation of smooth cracks in those same materials is perhaps less intuitive. Theoretical attempts have been made to understand when cracks will cleave crystals using both energetic arguments and lattice simulations (Deegan et al., 2003; Marder, 2004a, b). However, a fully consistent theoretical picture has not yet emerged.

The crack propagation law Eq. (59) provides an explicit prediction of when a crack will propagate along a cleavage plane, or smoothly in other directions. Restricting our discussion to two dimensions for simplicity, the surface energy in a crystalline material is expected to show a cusp behavior

$$\gamma(\theta) = \gamma_0(1 + \delta|\theta| + \cdots), \tag{69}$$

near a cleavage plane (and more generally near sets of equivalent low energy crystal planes imposed by symmetry), where θ measures the angle of the surface away from this plane, and to be a smooth differentiable function of θ for other orientations. In terms of the physical picture outlined in Section 2, this cusp behavior implies the presence of a finite Herring torque on any small extension of a crack at an infinitesimal angle away from a cleavage plane. Therefore, a crack will be essentially trapped along a cleavage plane until the Eshelby configurational torque is large enough to tilt the crack away from this plane. Restated in terms of the propagation law, Eq. (59) can be obeyed for small non-zero angles only when $|K_2|$ exceeds a threshold $K_2^{(c)}$ with

$$K_2^{(c)} = \frac{2\mu\gamma_0\delta}{(1-\nu)K_1} \quad \text{for } G \approx G_c. \tag{70}$$

Consequently, $|K_2|$ should exceed $K_2^{(c)}$ for a cleavage crack to change direction. Eq. (59) also implies that a crack will propagate smoothly for other orientations away from cleavage planes where the surface γ-plot is smooth. Relation (70) was proposed somewhat more heuristically in Marder (2004b).

One interesting prospect to test this prediction is to examine its consequences for thermal fracture in crystalline materials, where quasistatic oscillatory cracks have been studied under well-controlled experimental conditions. In particular, experiments have revealed that the onset of crack oscillations is markedly different in anisotropic and isotropic materials. In crystalline silicon wafers that cleave preferentially {1 1 0} planes, the onset of crack oscillations is delayed in comparison to an isotropic material and is accompanied by a discontinuous jump in oscillation amplitude consistent with a subcritical bifurcation (Deegan et al., 2003). In contrast, the onset of thermal crack oscillations in isotropic material has been shown to be supercritical in a recent phase-field modeling study, consistent with earlier experimental observations in glass (see Corson et al. (2008)) and earlier references to the experimental literature therein). The existence of a finite threshold equation (70) to escape a cleavage crack precludes a smooth transition to crack oscillations around a cleavage plane. One would therefore expect a subcritical bifurcation for the onset of crack oscillations if Eq. (59) is used in conjunction with a typical γ-plot for a crystalline material that exhibits cusps. However, a detailed study is clearly needed to validate this expectation and to make contact quantitatively with experiments.

6. Motion under pure antiplane shear

As recalled in the Introduction, the principle of local symmetry was first proposed in Barenblatt and Cherepanov (1961) for crack motion under pure antiplane shear. This particular case does not seem to have attracted much interest subsequently, presumably because rotation of the crack front is observed and fractures under mixed mode I–III loading are found to be unstable in three-dimensional isotropic materials (Sommer, 1969). The criterion of motion under antiplane shear could nonetheless have some importance for the development of the tridimensional instability. It is also conceivable that two-dimensional motion under pure mode III loading could be effectively realized in an appropriate anisotropic material, like for instance a thin layer of sintered glass beads. We therefore find it interesting to briefly examine this criterion for motion under pure antiplane shear with the formalism developed in the previous sections.

Since in a pure mode III motion, the displacement field reduces to its third component u_3 that is a purely scalar Laplacian field, the diverging stress distribution near the tip equation (3) is always symmetrical and produces no configurational force perpendicular to the crack axis. Consequently, for propagation in an anisotropic material, the propagation law reduces simply to the condition that the Herring torque vanishes, $\gamma_\theta = 0$. This condition implies that in the limit of vanishing velocity, a quasistatic crack propagates in a direction that corresponds to a local minimum of the surface energy; it can be argued that propagation in a direction of maximal γ is unstable because the configurational torque amplifies small departures from this direction. Furthermore, for finite velocity, the dissipative force perpendicular to

the crack axis, $F_2^{(dis)}$, also vanishes since the phase-field profile must be symmetrical about the crack axis for a direction where $\gamma_\theta = 0$.

For propagation in an isotropic material, the situation is more subtle than for the mode I/II case. The evaluation of the contour integral that is the direct analog for mode III of the r.h.s. of Eq. (30) (or equivalently Eq. (38)), gives only a non-vanishing force perpendicular to the crack axis if the subdominant antisymmetrical contribution of the stress distribution (i.e., the second term on the r.h.s. of Eq. (3)) is included. This force is proportional to $K_3 A_2 \sqrt{R}$, where R is the radius of the integration contour around the crack tip, where the square-root behavior follows from dimensional analysis. This force vanishes if $A_2 = 0$, thereby suggesting that the original formulation of the principle of local symmetry for mode III might be applicable. However, our inner–outer matching procedure used to compute this force is predicated on choosing R much larger than the scale of the process zone but vanishingly small on the outer scale of the system size set by material boundaries. Therefore, the magnitude of this force is left undetermined in the present analysis. Further work is therefore needed to determine if the inner and outer scales can be clearly separated for pure antiplane shear and if $A_2 = 0$ can rigorously serve as a local condition to predict crack paths in isotropic material.

Additional insight into this question can be gained by repeating the analysis of Section 2 for a small extension δl of a mode III crack. The analogous expression for the SIF at the tip of the extended crack is $K_3^* = K_3 - b\mu A_2 \sqrt{\delta l}\delta\theta$ to linear order in $\delta\theta$ (Sih, 1965) where b is a numerical constant, and hence $G_\theta(0) \sim K_3 A_2 \sqrt{\delta l}$. One important difference with plane loading is the square-root dependence of $G_\theta(0)$ on the crack extension length, which is also reflected in the $\sqrt{R}$ dependence of the integral just mentioned above, which yields the configurational force perpendicular to the crack tip for mode III. Since the only natural cut-off for the crack extension length on the outer scale of the system is the size ξ of the process zone, this result seems to imply that $G_\theta(0) \sim K_3 A_2 \sqrt{\xi}$ up to a numerical prefactor. It also yields the local symmetry condition $A_2 = 0$ in the isotropic limit, where the symmetry of the phase-field profile makes the dissipative force $F_2^{(dis)}$ vanish.

7. Numerical simulations and tests

We first focus here on testing relation (59) between K_2 at a crack tip and the derivative of the surface energy, in the case of plane strain. We numerically compute the extension of a preexisting straight crack as described by the phase-field equation (19) and with the surface energy (18). For a pure mode I loading of the preexisting crack and an anisotropic surface energy, Eq. (59) predicts that the growth of a kinked extension takes place at an angle θ such that K_2 is adequate at the growing tip. More explicitly, on the one hand, Eq. (45) gives $\tilde{K}_2$ at the kink tip as

$$\tilde{K}_2 = F_{21}(\theta) K_1 \simeq K_1 \frac{\theta}{2}, \tag{71}$$

where the second equality is valid for small angles. Therefore, one obtains for small angles,

$$-2\alpha \tilde{K}_1 \tilde{K}_2 \simeq \alpha K_1^2 \theta, \tag{72}$$

since $\tilde{K}_1$ is equal to K_1 at dominant order in θ (Eq. (45)). On the other hand, the surface energy (18) gives

$$-2\gamma_\theta(0) = \varepsilon \gamma_0. \tag{73}$$

Eq. (59), which translates in the equality of the l.h.s. of Eqs. (72) and (73), simplifies for G close to Griffith threshold when $\alpha K_1^2 \simeq 2\gamma_0$. Then, it simply gives for the initial angle θ of the kink crack,

$$\theta = \frac{\varepsilon}{2}, \tag{74}$$

which is strictly valid for small angle ($\varepsilon \ll 1$) in the limit $G \to G_c$. For larger ε, the kink angle predicted by force-balance can be computed by using the series expansion for the $F_{ij}(\theta)$'s of Amestoy and Leblond (1992), as explained before (Eqs. (64) and (65)).

These predictions were tested numerically. Eq. (19) was solved by using an Euler explicit scheme to integrate the phase-field evolution and a successive over relaxation (SOR) method to calculate the quasistatic displacement fields u_1 and u_2 at each time step. We used as initial condition a straight horizontal crack of length $2W$ centered in a strip of length $4W$ horizontally and $2W$ vertically, with fixed values of u_1 and u_2 on the strip boundaries that correspond to the singular stress fields defined by Eq. (1) for prescribed values of K_1 and K_2. We used $\lambda/\mu = 1$ [$\alpha = 3/(8\mu)$], $\mathscr{E}_c/\mu = \frac{1}{2}$, a grid spacing $\Delta x_1 = \Delta x_2 = 0.1\xi$, and $W = 50\xi$, where the process zone size $\xi \equiv \sqrt{\kappa/(2\mathscr{E}_c)}$. We checked that the results were independent of width and grid spacing.

We first verified that, in the isotropic limit, the kink angle was well predicted by the local symmetry condition $K_2^* = 0$, which implies that $\theta \approx -2K_2/K_1$. Then, for the anisotropic case, Eq. (18), we chose $K_2 = 0$ and K_1 close to the onset of propagation. Namely, we chose $\Lambda^2 = \alpha K_1^2/2\gamma_0$ in the range of 1.1–1.2 (i.e., 10–20% above the propagation threshold of a horizontal crack). The kink angles were found to be independent of Λ within this range to numerical accuracy of the phase-field simulations such that the results can be meaningfully compared to the theoretical predictions of the force-balance condition at the onset of propagation. The results for the kink angles observed for several simulations with different magnitudes of the surface energy anisotropy ε are shown in Fig. 5. The prediction of the force-balance condition (74) is seen to be in good quantitative agreement with the results of the phase-field simulations.

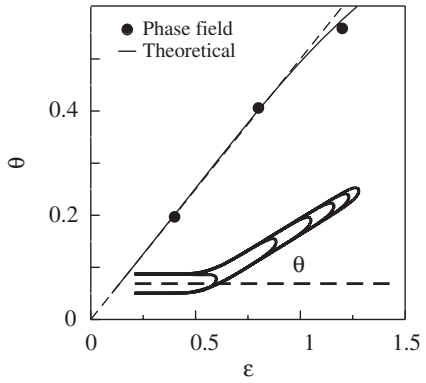

Fig. 5. Kink angle θ vs. surface energy anisotropy ε for plane strain and the surface energy anisotropy $\gamma(\theta)$ given by Eq. (18), as predicted by force-balance for small angle (analytical prediction $\theta = \varepsilon/2$ and thin dashed line) and for arbitrary angle (numerically calculated solid line), and as extracted from phase-field simulations (filled circles). Inset: phase-field simulation showing $\phi = \frac{1}{2}$ contours equally spaced in time for $\varepsilon = 1.2$ with the original crack axis (thick dashed line). The simulations were carried out in a $4W \times 2W$ strip with $W/\xi = 50$ with fixed displacement boundary condition corresponding to singular stress fields around the initial horizontal crack, $K_1 \neq 0$ and $K_2 = 0$, and $\Delta x_1 = \Delta x_2 = 0.1$.

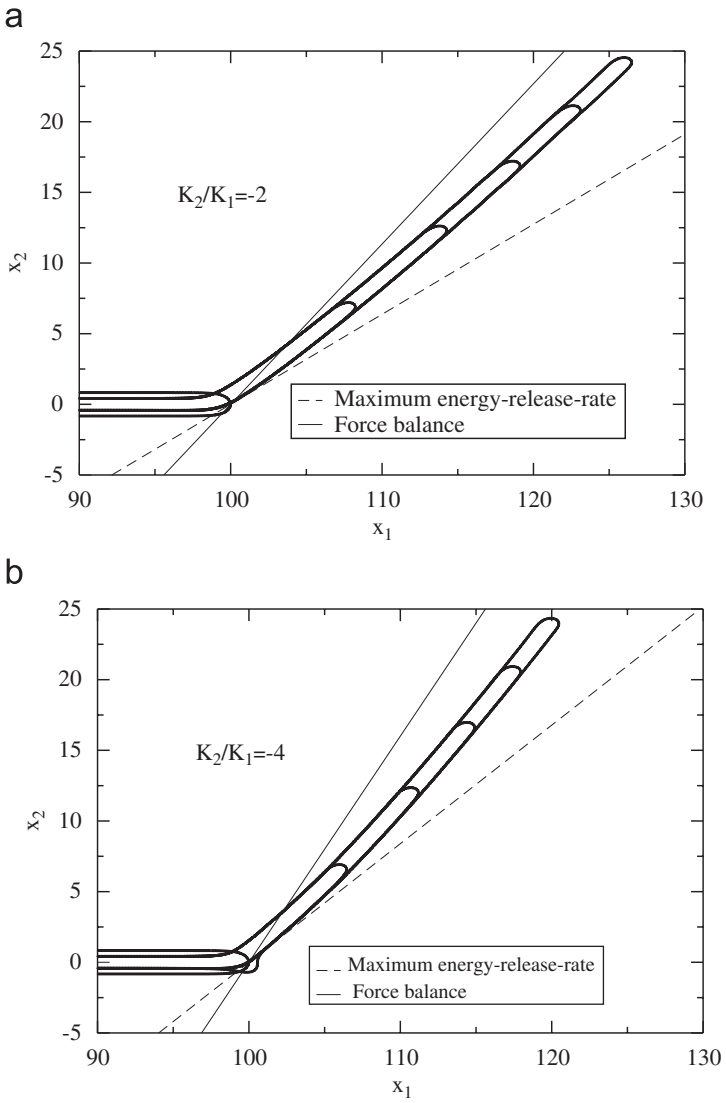

Fig. 6. Comparison of phase-field simulations in a $4W \times 2W$ strip with $W/\xi = 100$ and predictions of the maximum energy-release-rate criterion and the force-balance condition for the anisotropic surface energy $\gamma(\theta)$ given by Eq. (68). The phase-field results correspond to $\phi = \frac{1}{2}$ contours at equal intervals of time. The predictions of the maximum energy-release-rate criterion and the force-balance condition are represented by straight dashed and solid lines, respectively, passing through the initial position of the crack tip, and with slope $\tan\theta$ where θ is the kink angle; x_1 and x_2 are measured in units of ξ. Only a small region of the strip with the kink is shown. In (a) $K_2/K_1 = -2$, and $\theta_{mer} \approx 33^\circ$ ($\theta_{fb} \approx 48^\circ$) for maximum energy-release-rate (force-balance). In (b) $K_2/K_1 = -4$, and $\theta_{mer} \approx 34^\circ$ ($\theta_{fb} \approx 58^\circ$) for maximum energy-release-rate (force-balance).

In this first set of simulations, the predictions of the force-balance condition derived in the present paper and of the previously proposed maximum energy-release-rate criterion are close ($\sim 0.5^\circ$ for the largest tested anisotropy). Hence, they cannot be distinguished with our numerical accuracy. A second set of simulations was thus run with the anisotropic surface energy $\gamma(\theta)$ defined by Eq. (68), a case for which the two criteria give significantly different predictions of kink angles as explained in Section 5.3 and Fig. 4. Simulations were carried out for two different ratios of SIF $K_2/K_1 = -2$ and -4. The initial condition consisted of a W long horizontal crack in a $4W \times 2W$ strip. Fixed displacements u_1 and u_2 corresponding to the singular stress fields were imposed on the strip boundaries and the same grid resolution $\Delta x_1 = \Delta x_2 = 0.1\xi$ was used. Simulations were carried out as before for loads close to the onset of propagation for comparison with the theoretical predictions.

The results are compared to the predictions of the maximum energy-release-rate criterion and force-balance condition in Fig. 6. For both ratios of K_2/K_1, the kink emerges initially from the parent straight crack with an angle close to the one predicted by maximum energy-release-rate. Then, as it propagates further, the crack turns smoothly counterclockwise with a curvature independent of the box size, as explained below, and thus determined by the length scale ξ of the process zone, yielding a slightly curved crack path that is expected to approach asymptotically the kink angle predicted by force-balance. We note, however, that an accurate quantitative determination of this asymptotic kink angle is made extremely difficult by two opposite constraints. On the one hand, the strip width must be much larger than the kink length δl, in order to avoid finite-size effects induced by the outer boundaries, which curves the crack path. On the other hand, the kink length must itself be much larger than the process zone length scale ξ for the force-balance condition to hold. The phase-field simulations shown in Fig. 6 represent our best attempt to satisfy these stringent constraints ($W \gg \delta l \gg \xi$). We have checked with simulations in a twice larger system that the crack curvature in Fig. 6 is independent of finite-size effects induced by the outer boundaries. However, even larger scale simulations would be needed to accurately determine the asymptotic kink angle. The present simulations shown in Fig. 6 nonetheless give a clear example where the maximum energy-release-rate criterion fails to predict kink angles in an anisotropic material with mode I+II loading. This example is to be contrasted with the isotropic case extensively studied in the literature, or the case of Fig. 5 with a different surface energy anisotropy and pure mode I loading, where the two criteria give practically indistinguishable predictions.

Let us now turn to the issue of the "forbidden" gap plotted in Fig. 4C between the threshold loads for propagation given by the maximum energy-release-rate and force-balance conditions, which was explored in Section 5.3. Macroscopic kink cracks cannot exist in the phase-field model for angles that correspond to maximum energy-release-rate, as clearly validated by the simulations in Fig. 6, but only for angles that satisfy force-balance. Thus only the threshold load dictated by force-balance should generally be expected to have predictive value for experimentally observed crack paths on macroscopic length scales. It is conceivable that details on the process zone length scale (i.e. in the present context, details of the phase-field formulation) determine whether macroscopic kinks grow exactly at this threshold or only appear at a higher threshold with a finite velocity, in a subcritical way. In any case, kinks inside the "forbidden gap" should stay confined to the process zone length scale since they are below the force-balance threshold load. For the case $K_2/K_1 = -4$ in the above example, $\Lambda_{fb} = (\alpha K_1^2/(2\gamma_0)^{1/2} \approx 0.196$ ($\Lambda_{mer} \approx 0.193$) which is in good agreement with the threshold value ≈ 0.205 obtained by varying Λ in the phase-field simulations to determine the onset of kink propagation. These two thresholds cannot be compared more accurately given that the surface energy in the present finite-difference implementation of the phase-field equations differs by a few percents from its analytically predicted value and that the kinks have a finite length on the process zone length scale.

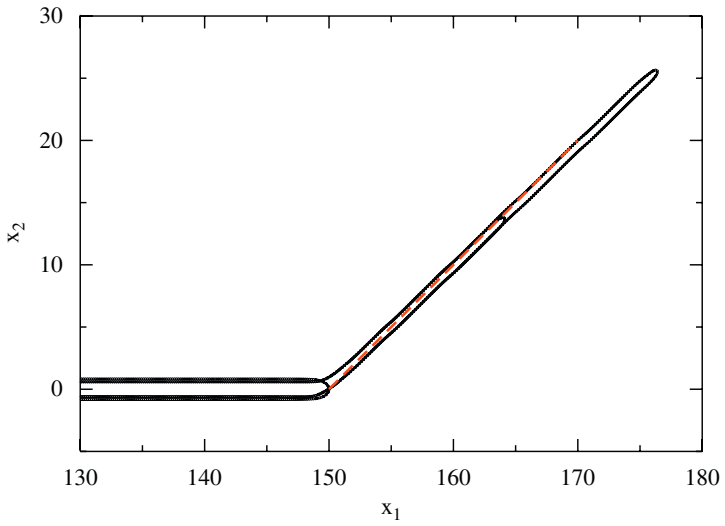

Fig. 7. Phase-field simulation for pure antiplane shear for $\varepsilon = 1.8$ ($\phi = \frac{1}{2}$ contours are equally spaced in time). The dashed line is a guide to the eye for the 45° kink angle predicted by the vanishing torque condition $\gamma_\theta = 0$.

Finally, we have also tested our prediction for pure mode III cracks. We used the same phase-field model with the anisotropy form of $\gamma(\theta)$ defined by Eq. (18), albeit with the strain energy corresponding to pure antiplane shear,

$$\mathscr{E}_{strain} = \frac{\mu}{2}[(\partial_1 u_3)^2 + (\partial_2 u_3)^2]. \tag{75}$$

We used as initial condition a straight horizontal crack of length $3W$ centered in a strip of length $6W$ horizontally (along the x_1-axis) and $2W$ vertically together with $\mathscr{E}_c/\mu = \frac{1}{2}$, the anisotropy $\varepsilon = 1.8$, a grid spacing $\Delta x_1 = \Delta x_2 = \xi/6$, a half strip width $W = 50\xi$, and a fixed displacement $u_3 = 11.313\xi$ on the $x_2 = \pm W$ boundaries corresponding to a crack slightly above the Griffith threshold, where as before the process zone size $\xi \equiv \sqrt{\kappa/(2\mathscr{E}_c)}$.

The results of this simulation shown in Fig. 7 confirm that a crack centered initially in the strip with its axis parallel to the $\theta = 0$ direction, kinks at a 45° angle ($\theta = \pi/4$) that is consistent with the analytical prediction $\gamma_\theta = 0$ for mode III in an anisotropic material.

Fracture in the phase-field model that we have considered here is a reversible process in the sense that cracks can (and do) heal when stresses are removed. This can also be observed in some experiments under very clean conditions when no alterations of exposed surfaces follow breaking. Nonetheless, this is sometimes considered a troublesome feature since it does not occur in more usual conditions. One could think of introducing irreversibility in a"physical way" by adding another field to mimick surface oxydation. In a simpler but more *ad hoc* fashion, one can only accept evolutions that decrease the value of the phase field. To assess the importance of reversibility on our results, the numerical simulations above for modes I/II and III were redone with this second scheme ((i.e. taking Eq. (19)) as written when $\partial_t\phi < 0$ and otherwise replacing it by $\partial_t\phi = 0$). While the loads corresponding to the onset of crack propagation where found to be very slightly different for reversible and irreversible dynamics (Λ_{fb} is a few percent larger in the irreversible case), the macroscopic crack paths were found to be essentially identical for the same load above the onset of propagation for both cases. In particular, the $\phi = \frac{1}{2}$ phase-field contours of Figs. 5 and 6 superimpose perfectly for the two sets of simulations with and without reversible dynamics. This insensitivity of macroscopic crack paths to the introduction of irreversibility does not appear surprising since our derivation of crack propagation laws for modes I/II and III rely on the *existence* of propagating solutions for which $\partial_t\phi < 0$.

8. Conclusion

We have analyzed here the laws of quasistatic crack tip motion within the phase-field framework. The analysis provides a derivation of the principle of local symmetry and of its generalization to anisotropic materials. It also underlines the role of the configurational force perpendicular to the crack tip direction. The results can be interpreted physically as a simple force-balance condition. The variational character of the phase-field equations of motion played an important role in the derivation of the equations for the crack tip. It directly allowed us in Section 5 to define a generalization of Eshelby tensor that includes the phase field and short-scale physics while keeping its divergenceless property. Its role in the derivation of Section 4 may be less central from a conceptual point of view but the self-adjointness of the linear operator allowed the obtention of explicit formulas. In any case, it should be noted that direct link to energy considerations *à la* Griffith require a variational model.

Several questions appear worth of further investigations. First, it would be worthwhile to extend phase-field simulations to larger system sizes for cases where the force-balance condition and the maximum energy-release-rate criterion give strikingly different predictions of kink angle, as in the example of Fig. 6. In particular, it would be interesting to understand how, in this case, forces on the process-zone scale cause the crack to initially gently curve, independently of macroscopic length scales, before it approaches its asymptotic kink angle predicted by the force-balance condition; and, why, in cases where the force-balance condition and the maximum energy-release-rate criterion give similar predictions, kinks are straight even on the process zone length scale as in the example of Fig. 5. This goes beyond what we have analytically studied here and merits further scrutiny. Second, it would be interesting to study the effects of dissipative forces on the process zone scale for finite crack velocity and to study the role of inertia in dynamics, as opposed to quasistatic, fracture. Third, for pure mode III cracks, even if they are not realized under most experimental conditions, the applicability of the principle of local symmetry ($A_2 = 0$) remains to be established on a firmer footing in the isotropic limit where the force perpendicular to the crack tip seems to depend on an arbitrary cut-off on the scale of the process zone. Fourth, the crack propagation laws have been here derived for a gradient formulation of the phase-field dynamics where failure is reversible. Even though our numerical simulations indicate that a simple *ad hoc* introduction of irreversibility (where the phase field can only decrease in time) does not alter crack paths, it is found to slightly alter the threshold load for propagation. Therefore, the role of irreversibility, and in particular the dependence on this threshold load on details of the process zone dynamics, is worth investigating more fully.

The phase-field energy is certainly another aspect that would benefit from further refinement. As written in Eqs. (15) and (19), it does not distinguish between compressive and extensive strains which is quite an unphysical feature. Note that this property is also shared by the variational formulation advocated by Francfort and Marigo (1998) (illustrated in numerical simulations of Bourdin et al. (2000), Fig. 4, in which it is referred to as sample interpenetration). Some remedies have been proposed (Henry and Levine, 2004) but have the disadvantage that they break the variational character of the

equations of motion. The development of more physically motivated and material adapted energies certainly appear as an interesting future endeavor.

The extension of the present analysis to three dimensions where fracture paths are geometrically more complex is another important future direction. Numerical simulations and preliminary analysis addressing this question will be reported elsewhere (Pons and Karma, 2008).

Finally, we hope that the results reported here will contribute to stimulate further experimental investigations of quasistatic crack motion in anisotropic media.

Acknowledgments

We thank M. Adda-Bedia, J.B. Leblond, A. Chambolle, G. Francfort and J.J. Marigo for valuable discussions and instructive comments. We are also grateful to E. Katzav and M. Adda-Bedia for allowing us to check our computation of the kinked crack functions F_{ij} against their numerically computed values. A.K. acknowledges the support of DOE Grant no. DE-FG02-07ER46400 and the hospitality of the Ecole Normale Supérieure in Paris where part of this work was completed.

Appendix A. The KKL phase-field model in one dimension

In this appendix, we recall the analysis of the KKL phase-field model in one dimension, that is the snap-back of a stretched elastic band, as described in Karma et al. (2001). In particular, the energy of the fractured state Eq. (A.22) provides the expression of the surface energy given in the main text. We also show how the fractured solution appears in one dimension in this model. For an elastic band of size $2L$, the elastically stretched state is the only allowed state when the total strain 2Δ is low enough. Above a critical total strain $2\Delta_c$ two other non-trivial solutions appear via a saddle-node bifurcation, one being dynamically stable and the other being unstable. At the bifurcation, both solutions have a higher energy than the elastically stretched state. However, the dynamically stable solution becomes energetically favored as compared to the elastically stretched state when the total strain becomes higher than $2\Delta_G\,(>2\Delta_c)$, which corresponds to the Griffith threshold in the model. This scenario is illustrated by numerical solution in Fig. A1. The unstable solution corresponds to the energy barrier (the Eyring state) that has to be overcome to create the fractured state and it provides the corresponding activation energy.

For a one-dimensional band, the KKL energy reads

$$E=\int_{-L}^{+L}\mathrm{d}y\left\{\frac{\kappa}{2}(\partial_y\phi)^2+g(\phi)\left[\left(\frac{\lambda}{2}+\mu\right)(\partial_y u)^2-\mathscr{E}_c\right]+\mathscr{E}_c\right\}, \tag{A.1}$$

with the function g monotonically increasing from $g(0)=0$ in the fully broken state to $g(1)=1$ in the intact material with also $g'(1)=0$ to recover linear elasticity. Steady state solutions obey the equilibrium equation obtained by variation of

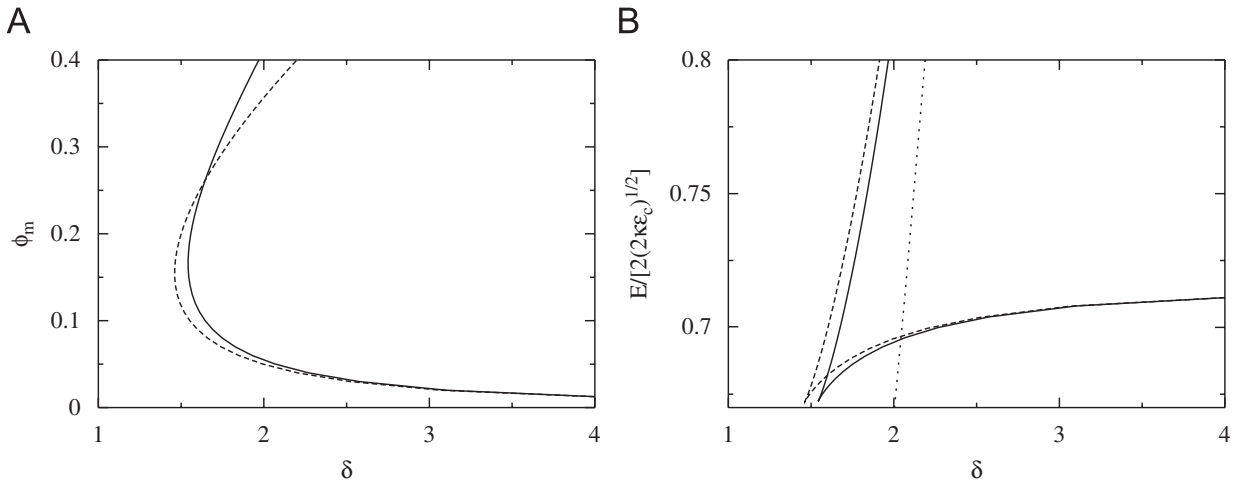

Fig. A1. (A) Minimum value ϕ_m of the phase field vs. adimensioned displacement $\delta=\Delta(\mu/\kappa)^{1/2}$ for a strip of adimensioned half-width $\ell=L(2\mathscr{E}_c/\kappa)^{1/2}=3$ (solid line) and in the limit of a large strip (dashed line), as given by Eq. (A.14) with $\ell=3$. For a given displacement $\delta>\delta_c$, there are two values of ϕ_m corresponding to two stationary solutions with the smallest value of ϕ_m for the stable one. (B) The energies E vs. δ for the two branches of solutions for the same band of $\ell=3$ (solid line), the lower branch corresponding to the stable fractured state. The asymptotic expression for a large band is also plotted using Eq. (A.20) with $\ell=3$ (dashed line). The two branches meet at a cusp, the generic behavior at a saddle-node bifurcation. The corresponding adimensioned energy $\delta^2/(2\ell)$ of the (half) elastically stretched band is also plotted (dotted line). It becomes larger than the energy of the stable fractured solution at Griffith threshold.

Eq. (A.1),

$$\kappa\partial_{yy}\phi = g'(\phi)\left[\left(\frac{\lambda}{2}+\mu\right)(\partial_y u)^2 - \mathscr{E}_c\right], \tag{A.2}$$

$$\partial_y[g(\phi)\partial_y u] = 0, \tag{A.3}$$

with the boundary conditions $u(\pm L) = \pm\Delta, \phi(\pm L) = 1$. The elastically stretched band $\phi = 1,\ u(y) = y\Delta/L$ is always a solution of Eqs. (A.2) and (A.3) and its energy is equal to the usual purely elastic one

$$E = (\lambda + 2\mu)\Delta^2/L. \tag{A.4}$$

In order to analyze the existence of other less obvious solutions of Eqs. (A.2) and (A.3), it is useful to note that Eq. (A.3) can be integrated once to obtain

$$\partial_y u = \sqrt{\frac{\mathscr{E}_c}{\lambda/2+\mu}}\frac{c}{g(\phi)}, \tag{A.5}$$

with c a constant yet to be determined. Eq. (A.5) allows the elimination of the strain field from the phase-field equation (A.2) which then reads

$$\kappa\partial_{yy}\phi = \mathscr{E}_c g'(\phi)\left[\frac{c^2}{g^2(\phi)} - 1\right]. \tag{A.6}$$

In a usual way, it is helpful to consider y as a fictitious time and to think of Eq. (A.6) as describing the motion of a point particle in the effective potential

$$V_{eff}(\phi) = \frac{c^2}{g(\phi)} + g(\phi). \tag{A.7}$$

With this analogy, a non-trivial solution of Eq. (A.6) corresponds to a particle that starts at "time" $y = -L$ from $\phi = 1$ with a negative velocity $\partial_y\phi < 0$, to reach a minimum $\phi = \phi_m$ at $y = 0$ where the "velocity" $\partial_y\phi$ vanishes; from this turning point it then follows the time-reversed motion and comes back to $\phi = 1$ at $y = +L$. The integrability of this one-dimensional motion gives the conservation law

$$\frac{\kappa}{\mathscr{E}_c}(\partial_y\phi)^2 + V_{eff}(\phi) = V_{eff}(\phi_m). \tag{A.8}$$

This allows us to express the energy (Eq. (A.1)) of the corresponding non-trivial solution as

$$E = \sqrt{2\kappa\mathscr{E}_c}\int_{\phi_m}^{1}\frac{\mathrm{d}\phi}{\sqrt{V_{eff}(\phi_m) - V_{eff}(\phi)}}[1 + V_{eff}(\phi_m) - 2g(\phi)]. \tag{A.9}$$

Two constraints determine the two unknown constants c and ϕ_m as a function of the dimensionless strip width ℓ and dimensionless total strain δ. First, the particle motion should take a total time $2L$ with

$$\ell = L\sqrt{2\mathscr{E}_c/\kappa} = \int_{\phi_m}^{1}\frac{\mathrm{d}\phi}{\sqrt{V_{eff}(\phi_m) - V_{eff}(\phi)}}. \tag{A.10}$$

Second, the overall integrated strain should equal the imposed displacement

$$\delta = \Delta\sqrt{(\lambda+2\mu)/\kappa} = c\int_{\phi_m}^{1}\frac{\mathrm{d}\phi}{g(\phi)\sqrt{V_{eff}(\phi_m) - V_{eff}(\phi)}}. \tag{A.11}$$

We analyze more specifically the case of a macroscopic strip of width $\ell \gg 1$.

We find it convenient to first consider the dependence of Eq. (A.10) on c. Since the sum of kinetic energy $[\kappa/(2\mathscr{E}_c)(\partial_y\phi)^2]$ and potential energy $[V_{eff}(\phi)]$ is constant along the particle trajectory (Eq. (A.8), the initial potential energy is always lower than the potential energy at the return point where the kinetic energy vanishes), $V_{eff}(1) < V_{eff}(\phi_m)$. For a given ϕ_m, the time L spent by the particle during its motion increases as its initial velocity $|\partial_y\phi|$ decreases. It is thus maximal in the limit where $V_{eff}(1) = 1 + c^2$ tends towards $V_{eff}(\phi_m) = c^2/g(\phi_m) + g(\phi_m)$, that is in the limit $c^2 \to g(\phi_m)$. The time spent on the trajectory diverges logarithmically when c^2 approaches $g(\phi_m)$ (since g' has a double zero at $\phi = 1$). Thus, for $\ell \gg 1$, c^2 is exponentially close to $g(\phi_m)$.

We consider now the integrated strain constraint, equation (A.11), and the determination of ϕ_m. It is helpful to rewrite Eq. (A.11) using Eq. (A.10) as

$$\delta = c\ell + c\int_{\phi_m}^{1}\mathrm{d}\phi\frac{1 - g(\phi)}{g(\phi)\sqrt{V_{eff}(\phi_m) - V_{eff}(\phi)}}. \tag{A.12}$$

Under this form, for large ℓ, as $c^2 \to g(\phi_m)$ the integral in Eq. (A.12) converges and c^2 can be replaced by $g(\phi_m)$ with an exponentially small error. Thus, one obtains

$$\delta \simeq g(\phi_m)^{1/2}\left\{\ell + \int_{\phi_m}^{1} \mathrm{d}\phi \sqrt{\frac{1-g(\phi)}{g(\phi)[g(\phi)-g(\phi_m)]}}\right\}. \tag{A.13}$$

The existence of solutions with $\delta \ll \ell$ imposes $g(\phi_m) \ll 1$ (since the integral term in Eq. (A.13) is clearly positive). When g behaves as $g(\phi) \sim a\phi^{\sigma}$ for small ϕ, equation (A.13) reduces to

$$\delta \simeq \sqrt{a}\phi_m^{\sigma/2}\ell + \frac{C_\sigma}{\sqrt{a}}\phi_m^{1-\sigma/2}, \tag{A.14}$$

where the constant C_σ can be expressed in term of the Euler B function as $C_\sigma = B(1-1/\sigma, \frac{1}{2})/\sigma$. The first term in Eq. (A.14) represents a contribution to the total displacement that is distributed over the whole sample, whereas the second one is a localized contribution coming from the center of the stretched band. If one wishes that some solutions can correspond to fractured bands, the second contribution should dominate the first. It should moreover be able to take values much larger than one (so than one can have localized solutions with $\delta \gg 1$). This clearly requires the exponent $1-\sigma/2$ to be negative and therefore that the function $g(\phi)$ be chosen so that $\sigma > 2$, as noted in Karma et al. (2001). A possible choice, made in the present work as in Karma et al. (2001), is to take $\sigma = 3$ (in addition to the requirements $g(1) = g'(1) = 0$) and

$$g(\phi) = 4\phi^3 - 3\phi^4. \tag{A.15}$$

For this specific choice, clearly $a = 4$ and $C_3 = B(\frac{2}{3}, \frac{1}{2})/3 \simeq 0.862$. For $\sigma > 2$, the r.h.s. of Eq. (A.14) has a minimum value δ_c that is reached for $\phi_m = \phi_c$ with

$$\phi_c^{\sigma-1} \simeq C_\sigma(\sigma-2)/(a\sigma\ell), \tag{A.16}$$

$$\delta_c \simeq \sqrt{a}\frac{2(\sigma-1)}{\sigma-2}\ell\phi_c^{\sigma/2} \sim \ell^{(\sigma-2)/2(\sigma-1)}, \tag{A.17}$$

or more simply for our specific choice of g with $\sigma = 3$, $\phi_c \simeq 0.268/\sqrt{\ell}$ and $\delta_c \simeq 1.11\ell^{1/4}$. For an adimensioned strain δ below δ_c no non-trivial solutions exist. Two coincident solutions appear at $\delta = \delta_c$ which separate into a stable lower energy solution and an unstable higher energy one when $\delta > \delta_c$ as shown in Fig. A1. The energies of the two solutions can be explicitly obtained in the limit $\ell \gg 1$. Eq. (A.9) can be rewritten as

$$\frac{E}{\sqrt{2\kappa\mathscr{E}_c}} = [V_{\mathit{eff}}(\phi_m) - 1]\ell + \int_{\phi_m}^{1} \frac{\mathrm{d}\phi}{\sqrt{V_{\mathit{eff}}(\phi_m) - V_{\mathit{eff}}(\phi)}} 2[1-g(\phi)], \tag{A.18}$$

where we have used expression (A.10) for the strip width ℓ. For a large ℓ, c^2 can be replaced by $g(\phi_m)$ with an exponentially small error to obtain

$$\frac{E}{\sqrt{2\kappa\mathscr{E}_c}} = g(\phi_m)\ell + 2\int_{\phi_m}^{1} \mathrm{d}\phi[1-g(\phi)]\sqrt{\frac{g(\phi)}{g(\phi)-g(\phi_m)}}. \tag{A.19}$$

Finally, in the whole regime of interest where $\delta \ll \ell$, the phase-field minimum value ϕ_m vanishes as a power of ℓ. With the small ϕ behavior $g(\phi) \sim a\phi^{\sigma}$, Eq. (A.19) simply reduces to

$$\frac{E}{\sqrt{2\kappa\mathscr{E}_c}} = a\phi_m^{\sigma}\ell - D_\sigma\phi_m + 2\int_0^1 \mathrm{d}\phi[1-g(\phi)], \tag{A.20}$$

where as above the constant D_σ can be expressed using Euler B function ($D_\sigma = (\sigma-2)C_\sigma$) and for $\sigma = 3$, $D_3 \simeq 0.862$. The asymptotic form (A.20) is already reasonably accurate for $\ell = 3$ as shown in Fig. A1.

As δ becomes much larger than δ_c, these two solutions correspond to the dominance of one of the two terms on the l.h.s. of Eq. (A.13).

For the stable solution, the localized contribution to the strain dominates so that

$$\delta \simeq \frac{C_\sigma}{\sqrt{a}}\phi_m^{1-\sigma/2}. \tag{A.21}$$

Thus, in this parameter regime, $\ell \gg 1$ and $\delta \gg \delta_c \gg 1$, ϕ_m tends toward zero. As a welcome consequence, the energy of the stable solution becomes independent of the strain and can be identified with twice the surface energy γ

$$E_s = 2\gamma = 2\sqrt{2\kappa\mathscr{E}_c}\int_0^1 \mathrm{d}\phi\sqrt{1-g(\phi)}. \tag{A.22}$$

For our specific choice of $g(\phi)$ (Eq. (A.15)) the numerical value of the integral is approximately 0.7165. As in Griffith's original theory, this stable solution becomes energetically favored as compared to the elastically stretched band when E_s becomes smaller than the purely elastic stretching energy (Eq. (A.4)), that is when $\Delta > \Delta_g = \sqrt{[2\gamma/(\lambda+\mu)]L}$ or equivalently for $\delta > \delta_g = 1.20\sqrt{\ell}$.

For the unstable solution, when δ becomes much larger than δ_c, one has simply

$$\delta \simeq \sqrt{a}\phi_m^{\sigma/2}\ell. \tag{A.23}$$

The corresponding energy is simply (Eqs. (A.20) and (A.22)),

$$E_u = 2\gamma + \sqrt{2\kappa\mathscr{E}_c}\frac{\delta^2}{\ell}, \tag{A.24}$$

since the term proportional to ϕ_m becomes subdominant with respect to the other two (and tends towards zero) when δ moves away from δ_c. In other terms, the energy of the unstable state is simply the energy of the elastically stretched band plus the energy necessary to create the two interfaces, as one could have intuitively guessed.

Finally, it is interesting to see how the profile of the fracture state depends on the total strain δ. The profile of a general solution is obtained from Eq. (A.6) as

$$\frac{y}{\xi} = \int_{\phi_m}^{\phi} \frac{\mathrm{d}\phi}{\sqrt{V_{eff}(\phi_m) - V_{eff}(\phi)}}, \tag{A.25}$$

with as before $\xi = \sqrt{\kappa/(2\mathscr{E}_c)}$ denotes the process zone scale. In the regime $\ell \gg 1$ and $\delta \gg 1$ (or equivalently $\phi_m \ll 1$) the phase-field profile on the process zone scale is independent of δ

$$\frac{y}{\xi} = \int_{0}^{\phi} \frac{\mathrm{d}\phi}{\sqrt{1 - g(\phi)}}. \tag{A.26}$$

This is not true for ϕ comparable to ϕ_m (in the regime $\ell \gg 1$ and $\delta \gg 1$) where Eq. (A.25) simplifies to

$$\frac{y}{\xi} = \phi_m \int_{1}^{\phi/\phi_m} \frac{\rho^{\sigma/2}\,\mathrm{d}\rho}{\sqrt{\rho^\sigma - 1}}. \tag{A.27}$$

In the same regime $\phi \sim \phi_m$, the strain field can be written as

$$u = \sqrt{\frac{\kappa}{\lambda + 2\mu}}\frac{\phi_m^{1-\sigma/2}}{\sqrt{a}}\int_{1}^{\phi/\phi_m} \frac{\mathrm{d}\rho}{\rho^{\sigma/2}\sqrt{\rho^\sigma - 1}} = \frac{\Delta}{C_\sigma}\int_{1}^{\phi/\phi_m} \frac{\mathrm{d}\rho}{\rho^{\sigma/2}\sqrt{\rho^\sigma - 1}}. \tag{A.28}$$

Comparison of Eqs. (A.27) and (A.28) shows that the variation of u is comparable to the total strain Δ (Eq. (A.21)) on a scale $\phi_m\xi$ much smaller than the process zone length. More precisely, for different strains Δ, the different scaled strain profiles u/Δ are given by a unique function of $y/(\phi_m\xi)$.

Appendix B. Variational equations and self-adjointness of linearized operators

The equilibrium phase-field equations considered in this paper are Euler–Lagrange equations coming from the variation of an energy density $\mathscr{E}$ where $\mathscr{E}$ depends on a set of fields ψ_α (here the elastic displacements and a scalar phase-field) and their spatial derivatives $\partial_j\psi_\alpha$,

$$\frac{\partial\mathscr{E}}{\partial\psi_\alpha} - \partial_j\frac{\partial\mathscr{E}}{\partial[\partial_j\psi_\alpha]} = 0. \tag{B.1}$$

We show here that quite generally for this type of equations, the allied linear operator is self-adjoint, a property that we used for obtaining the explicit formulae of Section 4.

Linearization of Eq. (B.1) around a solution $\psi_\alpha^{(0)}$ produces the linearized operator $\mathscr{L}$. It is defined by its action on a set of functions v_β as

$$\mathscr{L}_\alpha[\{v_\beta\}] = \frac{\partial^2\mathscr{E}}{\partial\psi_\alpha\partial\psi_\beta}v_\beta + \frac{\partial^2\mathscr{E}}{\partial\psi_\alpha\partial[\partial_j\psi_\beta]}\partial_j v_\beta - \partial_j\left\{\frac{\partial^2\mathscr{E}}{\partial\psi_\beta\partial[\partial_j\psi_\alpha]}v_\beta\right\} - \partial_j\left\{\frac{\partial^2\mathscr{E}}{\partial[\partial_k\psi_\beta]\partial[\partial_j\psi_\alpha]}\partial_k v_\beta\right\}. \tag{B.2}$$

Now it is easily seen using integration by parts that for two arbitrary sets of differentiable functions v_β and w_α, one has

$$\int \mathrm{d}x\; w_\alpha\mathscr{L}_\alpha[\{v_\beta\}] = \int \mathrm{d}x\; v_\alpha\mathscr{L}_\alpha[\{w_\beta\}] + \text{boundary terms}. \tag{B.3}$$

The relation clearly holds separately for the first and last term on the r.h.s. of Eq. (B.2) and comes from the interchange of the second and third term on using integration by parts. Thus, the linear operator $\mathscr{L}_\alpha$ is self-adjoint for the usual flat measure (here simply $\mathrm{d}x \equiv \mathrm{d}x_1\,\mathrm{d}x_2$ on the plane).

Appendix C. Explicit computations of zero-modes and solvability integrals

For the convenience of the reader, we provide below some details of our computations of solvability integrals and of the Eshelby tensor line integrals.

For plane strain, the explicit form (1) of the stress distribution near a crack tip is conveniently obtained from the Airy function χ which satisfies the biharmonic equation

$$\nabla^2(\nabla^2\chi) = 0. \tag{C.1}$$

In polar coordinates (r,Θ), χ is related to the strain tensor by

$$\sigma_{rr} = \frac{1}{r^2}\partial^2_{\Theta\Theta}\chi + \frac{1}{r}\partial_r\chi, \quad \sigma_{\Theta\Theta} = \partial^2_{rr}\chi \quad \text{and} \quad \sigma_{r\Theta} = \frac{1}{r^2}\partial_\Theta\chi - \frac{1}{r}\partial^2_{r\Theta}\chi. \tag{C.2}$$

For a crack along the x-axis, with its tip at $x=0$, the Airy function is determined by Eq. (C.1), together with zero traction boundary conditions on the fracture lips, $\sigma_{rr} = \sigma_{r\Theta} = 0$ for $\Theta = \pm\pi$. The most singular possibility compatible with a bounded elastic energy reads, in polar coordinates,

$$\chi = \frac{r^{3/2}}{3}\left\{\frac{K_1}{\sqrt{2\pi}}\left[3\cos\left(\frac{\Theta}{2}\right) + \cos\left(\frac{3\Theta}{2}\right)\right] - \frac{K_2}{\sqrt{2\pi}}\left[\sin\left(\frac{\Theta}{2}\right) + \sin\left(\frac{3\Theta}{2}\right)\right]\right\}. \tag{C.3}$$

The dominant divergent forms of the stress distribution follow by differentiation with the help of Eq. (C.2),

$$\begin{aligned}
\sigma_{rr} &= \frac{K_1}{\sqrt{2\pi r}}\left[\frac{5}{4}\cos\left(\frac{\Theta}{2}\right) - \frac{1}{4}\cos\left(\frac{3\Theta}{2}\right)\right] - \frac{K_2}{\sqrt{2\pi r}}\left[\frac{5}{4}\sin\left(\frac{\Theta}{2}\right) - \frac{3}{4}\sin\left(\frac{3\Theta}{2}\right)\right],\\
\sigma_{\Theta\Theta} &= \frac{K_1}{\sqrt{2\pi r}}\left[\frac{3}{4}\cos\left(\frac{\Theta}{2}\right) + \frac{1}{4}\cos\left(\frac{3\Theta}{2}\right)\right] - \frac{K_2}{\sqrt{2\pi r}}\left[\frac{3}{4}\sin\left(\frac{\Theta}{2}\right) + \frac{3}{4}\sin\left(\frac{3\Theta}{2}\right)\right],\\
\sigma_{r\Theta} &= \frac{K_1}{\sqrt{2\pi r}}\left[\frac{1}{4}\sin\left(\frac{\Theta}{2}\right) + \frac{1}{4}\sin\left(\frac{3\Theta}{2}\right)\right] + \frac{K_2}{\sqrt{2\pi r}}\left[\frac{1}{4}\cos\left(\frac{\Theta}{2}\right) + \frac{3}{4}\cos\left(\frac{3\Theta}{2}\right)\right].
\end{aligned} \tag{C.4}$$

The relation between the strain and stress tensors (Eq. (20)) and integration give the allied displacement field,

$$u_i = \frac{1}{4\mu}\sqrt{\frac{r}{2\pi}}[K_1 d_i^{\mathrm{I}} + K_2\, d_i^{\mathrm{II}}], \quad i = r,\Theta. \tag{C.5}$$

The mode I crack tip displacement functions d_i^{I} are given by

$$\begin{aligned}
d_r^{\mathrm{I}} &= (5-8\nu)\cos\left(\frac{\Theta}{2}\right) - \cos\left(\frac{3\Theta}{2}\right),\\
d_\theta^{\mathrm{I}} &= (-7+8\nu)\sin\left(\frac{\Theta}{2}\right) + \sin\left(\frac{3\Theta}{2}\right).
\end{aligned} \tag{C.6}$$

The corresponding mode II functions are

$$\begin{aligned}
d_r^{\mathrm{II}} &= (-5+8\nu)\sin\left(\frac{\Theta}{2}\right) + 3\sin\left(\frac{3\Theta}{2}\right),\\
d_\Theta^{\mathrm{II}} &= (-7+8\nu)\cos\left(\frac{\Theta}{2}\right) + 3\cos\left(\frac{3\Theta}{2}\right).
\end{aligned} \tag{C.7}$$

These expressions allow the explicit evaluation of the different integrals of Sections 4 and 5.

(i) *Solvability integrals*: For a vectorial field $\mathbf{u} = u_r\mathbf{e}_r + u_\Theta\mathbf{e}_\Theta$ the two components of the x-translation field $\mathbf{u}^{(x)} \equiv \partial_x\mathbf{u}$ are

$$\begin{aligned}
u_r^{(x)} &= \cos(\Theta)\partial_r u_r - \frac{\sin(\Theta)}{r}\partial_\Theta u_r + \frac{\sin(\Theta)}{r}u_\Theta,\\
u_\Theta^{(x)} &= \cos(\Theta)\partial_r u_\Theta - \frac{\sin(\Theta)}{r}\partial_\Theta u_\Theta - \frac{\sin(\Theta)}{r}u_r.
\end{aligned} \tag{C.8}$$

With these formulae, one can compute the two components of the x-translation field $\mathbf{u}^{(x;I)}$ associated to the mode I displacement field (Eqs. (C.5) and (C.6)),

$$\begin{aligned}
u_r^{(x;\mathrm{I})} &= \frac{K_1}{8\mu\sqrt{2\pi r}}[(7-8\nu)\cos(3\Theta/2) - 3\cos(\Theta/2)],\\
u_\Theta^{(x;\mathrm{I})} &= \frac{K_1}{8\mu\sqrt{2\pi r}}[(-5+8\nu)\sin(3\Theta/2) + 3\sin(\Theta/2)].
\end{aligned} \tag{C.9}$$

The corresponding strain tensor reads

$$\begin{aligned}
u_{rr}^{(x;I)} &= \partial_r u_r^{(x;I)} = -\frac{K_1}{16\mu\sqrt{2\pi}\,r^{3/2}}[(7-8\nu)\cos(3\Theta/2) - 3\cos(\Theta/2)],\\
u_{\Theta\Theta}^{(x;I)} &= \frac{1}{r}[u_r^{(x;I)} + \partial_\Theta u_\Theta^{(x;I)}] = -\frac{K_1}{16\mu\sqrt{2\pi}\,r^{3/2}}[(1-8\nu)\cos(3\Theta/2) + 3\cos(\Theta/2)],\\
u_{r\Theta}^{(x;I)} &= \frac{1}{2}[\partial_r u_\Theta^{(x;I)} + \partial_\Theta u_r^{(x;I)}] = -\frac{3K_1}{16\mu\sqrt{2\pi}\,r^{3/2}}[\sin(3\Theta/2) + \sin(\Theta/2)].
\end{aligned} \tag{C.10}$$

The two needed components of the allied stress tensor follow

$$\sigma_{rr}^{(x;\mathrm{I})} = \frac{K_1}{8\sqrt{2\pi}\, r^{3/2}}[-7\cos(3\Theta/2) + 3\cos(\Theta/2)],$$
$$\sigma_{r\Theta}^{(x;\mathrm{I})} = -\frac{3K_1}{8\sqrt{2\pi}\, r^{3/2}}[\sin(3\Theta/2) + \sin(\Theta/2)]. \tag{C.11}$$

With these explicit expressions, one can evaluate the solvability integrals for the perturbed displacement field $u_i^{(1)}$,

$$u_i^{(1)} = \frac{1}{4\mu}\sqrt{\frac{r}{2\pi}}[\delta K_1\, d_i^{\mathrm{I}} + \delta K_2\, d_i^{\mathrm{II}}], \quad i = r, \Theta. \tag{C.12}$$

With Eqs. (C.4), (C.9) and (C.6), (C.11), one obtains for the two integrals

$$\int \mathrm{d}s_j u_i^{(1)}\sigma_{ij}^{(x;\mathrm{I})} = \int \mathrm{d}s_j\left[\frac{1}{4\mu}\sqrt{\frac{r}{2\pi}}\delta K_1\, d_i^{I}\sigma_{ij}^{(x;\mathrm{I})}\right] = \frac{K_1\,\delta K_1}{8\mu}[5 - 6\nu],$$
$$\int \mathrm{d}s_j u_i^{(x;\mathrm{I})}\sigma_{ij}^{(1)} = \frac{K_1\delta K_1}{8\mu}[-3 + 2\nu], \tag{C.13}$$

where $\sigma_{ij}^{(1)}$ is the perturbation of the stress tensor corresponding to $u_i^{(1)}$. It is given by the mode I part of Eq. (C.4) with K_1 and K_2 replaced by δK_1 and δK_2. For symmetry reasons, only the mode I part of $u_i^{(1)}$ and $\sigma_{ij}^{(1)}$ contribute to the integrals. Subtracting the two equations (C.13), one finally obtains

$$\int \mathrm{d}s_j[u_i^{(x;\mathrm{I})}\sigma_{ij}^{(1)} - u_i^{(1)}\sigma_{ij}^{(x;\mathrm{I})}] = -\frac{K_1\,\delta K_1}{\mu}[1 - \nu], \tag{C.14}$$

which is Eq. (27) of the main text.

The corresponding expressions for a y-translation field $\mathbf{u}^{(y)} \equiv \partial_y \mathbf{u}$ associated to a vectorial field $\mathbf{u} = u_r\mathbf{e}_r + u_\Theta\mathbf{e}_\Theta$ are

$$u_r^{(y)} = \sin(\Theta)\partial_r u_r + \frac{\cos(\Theta)}{r}\partial_\Theta u_r - \frac{\cos(\Theta)}{r}u_\Theta,$$
$$u_\Theta^{(y)} = \sin(\Theta)\partial_r u_\Theta + \frac{\cos(\Theta)}{r}\partial_\Theta u_\Theta + \frac{\cos(\Theta)}{r}u_r. \tag{C.15}$$

This gives for the two components of the y-translation field $\mathbf{u}^{(y;\mathrm{I})}$ associated to the mode I displacement field of Eq. (C.6)

$$u_r^{(y;\mathrm{I})} = \frac{K_1}{8\mu\sqrt{2\pi r}}[(7 - 8\nu)\sin(3\Theta/2) - \sin(\Theta/2)],$$
$$u_\Theta^{(y;\mathrm{I})} = \frac{K_1}{8\mu\sqrt{2\pi r}}[(5 - 8\nu)\cos(3\Theta/2) - \cos(\Theta/2)], \tag{C.16}$$

with the corresponding strain tensor

$$u_{rr}^{(y;\mathrm{I})} = -\frac{K_1}{16\mu\sqrt{2\pi}r^{3/2}}[(7 - 8\nu)\sin(3\Theta/2) - \sin(\Theta/2)],$$
$$u_{\Theta\Theta}^{(y;\mathrm{I})} = -\frac{K_1}{16\mu\sqrt{2\pi}r^{3/2}}[(1 - 8\nu)\sin(3\Theta/2) + \sin(\Theta/2)],$$
$$u_{r\Theta}^{(y;\mathrm{I})} = \frac{K_1}{16\mu\sqrt{2\pi}r^{3/2}}[3\cos(3\Theta/2) + \cos(\Theta/2)], \tag{C.17}$$

and stress tensor

$$\sigma_{rr}^{(y;\mathrm{I})} = \frac{K_1}{8\sqrt{2\pi}\, r^{3/2}}[-7\sin(3\Theta/2) + \sin(\Theta/2)],$$
$$\sigma_{r\Theta}^{(y;\mathrm{I})} = \frac{K_1}{8\sqrt{2\pi}\, r^{3/2}}[3\cos(3\Theta/2) + \cos(\Theta/2)]. \tag{C.18}$$

This gives for the two integrals of interest

$$\int \mathrm{d}s_j\, u_i^{(y;\mathrm{I})}\sigma_{ij}^{(1)} = \frac{K_1K_2}{8\mu}[5 - 6\nu],$$
$$\int \mathrm{d}s_j\, u_i^{(1)}\sigma_{ij}^{(y;\mathrm{I})} = \frac{K_1K_2}{8\mu}[-3 + 2\nu], \tag{C.19}$$

where only $\sigma_{ij}^{(1)}$ and $u_i^{(1)}$, the mode II parts of the perturbed stress tensor $\sigma_{ij}^{(1)}$ and displacements fields $u_i^{(1)}$ (Eq. (C.12)) contribute to the integrals.

One finally obtains for the difference of the two integrals of Eq. (C.19)

$$\int \mathrm{d}s_j[u_i^{(y;\mathrm{I})}\sigma_{ij}^{(1)} - u_i^{(1)}\sigma_{ij}^{(y;\mathrm{I})}] = \frac{K_1 K_2}{\mu}[1-\nu], \tag{C.20}$$

which is Eq. (30) of the main text.

(ii) *Components of the configurational force on the crack tip*: The two line integrals (Eq. (38)) giving the two components of the configurational force on the crack tip can be directly evaluated with the help of the above results.

$$f_i^{(conf)} = \int_{A\to B} \mathrm{d}s\, T_{ij}^E n_j = \int_{A\to B} \mathrm{d}s[\mathscr{E}_{strain} n_i - \sigma_{jk} u_k^{(i)}], \tag{C.21}$$

where $\mathbf{u}^{(i)} \equiv \partial_i \mathbf{u}$ is the translation field in the direction i ($i = x, y$), with modes I and II components included

$$u_k^{(i)} = u_k^{(i,\mathrm{I})} + u_k^{(i,\mathrm{II})}. \tag{C.22}$$

The mode I components $u_k^{(i,\mathrm{I})}$ are given by Eqs. (C.9) and (C.16). A similar computation gives their mode II components with the help of Eqs. (C.5), (C.7) and (C.8)

$$\begin{aligned} u_r^{(x;\mathrm{II})} &= \frac{K_2}{8\mu\sqrt{2\pi r}}[(-7+8\nu)\sin(3\Theta/2) + \sin(\Theta/2)], \\ u_\Theta^{(x;\mathrm{II})} &= \frac{K_2}{8\mu\sqrt{2\pi r}}[(-5+8\nu)\cos(3\Theta/2) + \cos(\Theta/2)] \end{aligned} \tag{C.23}$$

and

$$\begin{aligned} u_r^{(y,\mathrm{II})} &= \frac{K_2}{8\mu\sqrt{2\pi r}}[(7-8\nu)\cos(3\Theta/2) + 5\cos(\Theta/2)], \\ u_\Theta^{(y,\mathrm{II})} &= \frac{K_2}{8\mu\sqrt{2\pi r}}[(-5+8\nu)\sin(3\Theta/2) - 5\sin(\Theta/2)]. \end{aligned} \tag{C.24}$$

With these formulae and the stress tensor expression Eq. (C.4), one obtains

$$\begin{aligned} \int_{-\pi}^{+\pi} r\,\mathrm{d}\Theta[\sigma_{rr}u_r^{(x)} + \sigma_{r\Theta}u_\Theta^{(x)}] &= \frac{1}{8\mu}[K_1^2(-3+2\nu) + K_2^2(-5+6\nu)], \\ \int_{-\pi}^{+\pi} r\,\mathrm{d}\Theta[\sigma_{rr}u_r^{(y)} + \sigma_{r\Theta}u_\Theta^{(y)}] &= \frac{1}{4\mu}K_1K_2(3-2\nu). \end{aligned} \tag{C.25}$$

Furthermore, with $\mathscr{E}_{strain} = (\sigma_{ij}\sigma_{ij} - \nu\sigma_{ii}\sigma_{jj})$ and the stress tensor expression Eq. (C.4), one obtains

$$\int_{-\pi}^{+\pi} r\,\mathrm{d}\Theta\cos(\Theta)\mathscr{E}_{strain} = \frac{1}{8\mu}(K_1^2 - K_2^2)(1-2\nu), \tag{C.26}$$

$$\int_{-\pi}^{+\pi} r\,\mathrm{d}\Theta\sin(\Theta)\mathscr{E}_{strain} = -\frac{1}{4\mu}K_1K_2(1-2\nu). \tag{C.27}$$

Substraction of Eq. (C.25) from Eq. (C.26) gives the usual expression of $F_1^{(conf)}$,

$$F_1^{(conf)} = \int_{-\pi}^{+\pi} \mathrm{d}\Theta[\cos(\Theta)\mathscr{E}_{strain} - \sigma_{rr}u_r^{(x)} - \sigma_{r\Theta}u_\Theta^{(x)}] = \frac{1-\nu}{2\mu}(K_1^2 + K_2^2), \tag{C.28}$$

as given in Eq. (40) in the main text.

The other component of the configurational force $F_2^{(conf)}$ is similarly obtained by subtracting Eq. (C.25) from Eq. (C.27),

$$F_2^{(conf)} = \int_{-\pi}^{+\pi} \mathrm{d}\Theta[\sin(\Theta)\mathscr{E}_{strain} - \sigma_{rr}u_r^{(y)} - \sigma_{r\Theta}u_\Theta^{(y)}] = -\frac{1-\nu}{\mu}K_1K_2, \tag{C.29}$$

which is Eq. (41) of the main text.

References

Adda-Bedia, M., Arias, R., Ben Amar, M., Lund, F., 1999. Generalized Griffith criterion for dynamic fracture and the stability of crack motion at high velocities. Phys. Rev. E 60, 2366–2376.

Ambrosio, L., Tortorelli, V., 1990. Approximation of functionals depending on jumps by elliptic functionals via gamma-convergence. Commun. Pure Appl. Math. 43 (8), 999–1036.

Amestoy, M., Leblond, J., 1992. Crack path in plane situations. 2. Detailed form of the expansion of the stress intensity factors. Int. J. Solids Struct. 29 (4), 465–501.

Aranson, I., Kalatsky, V., Vinokur, V., 2000. Continuum field description of crack propagation. Phys. Rev. Lett. 85, 118–121.

Barenblatt, G., Cherepanov, G., 1961. On brittle cracks under longitudinal shear. PMM 25, 1110–1119.

Bourdin, B., Francfort, G., Marigo, J., 2000. Numerical experiments in revisited brittle fracture. J. Mech. Phys. Solids 48 (4), 797–826.

Brener, E.A., Marchenko, V.I., 1998. Surface instabilities in cracks. Phys. Rev. Lett. 81, 5141–5144.

Broberg, K.B., 1999. Cracks and Fracture. Academic Press, San Diego.

Corson, F., Adda-Bedia, M., Henry, H., Katzav, E., 2008. Thermal fracture as a framework for crack propagation law. cond-mat.mtrl-sci 0801.2101.
Cotterell, B., Rice, J., 1980. Slightly curved or kinked cracks. Int. J. Fract. 16 (2), 155–169.
Deegan, R., Chheda, S., Patel, L., Marder, M., Swinney, H., Kim, J., de Lozanne, A., 2003. Wavy and rough cracks in silicon. Phys. Rev. E 67, 066209.
Eastgate, L., Sethna, J., Rauscher, M., Cretegny, T., Chen, C., Myers, C., 2002. Fracture in mode I using a conserved phase-field model. Phys. Rev. E 65, 036117.
Eshelby, J., 1951. The force on an elastic singularity. Philos. Trans. Roy. Soc. (London) A 244 (877), 87–112.
Eshelby, J., 1975. Elastic energy-momentum tensor. J. Elasticity 5 (3–4), 321–335.
Francfort, G., Marigo, J., 1998. Revisiting brittle fracture as an energy minimization problem. J. Mech. Phys. Solids 46 (8), 1319–1342.
Goldstein, R., Salganik, R., 1974. Brittle-fracture of solids with arbitrary cracks. Int. J. Fract. 10 (4), 507–523.
Griffith, A., 1920. The phenomena of rupture and flows in solids. Philos. Trans. Roy. Soc. (London) A 221, 163–198.
Gurtin, M., Podio-Guidugli, P., 1998. Configurational forces and a constitutive theory for crack propagation that allows for kinking and curving. J. Mech. Phys. Solids 46 (8), 1343–1378.
Hakim, V., Karma, A., 2005. Crack path prediction in anisotropic brittle materials. Phys. Rev. Lett. 95, 235501.
Hauch, J., Holland, D., Marder, M., Swinney, H., 1999. Dynamic fracture in single crystal silicon. Phys. Rev. Lett. 82, 3823–3826.
Henry, H., 2008. Study of the branching instability using a phase field model of inplane crack propagation. Europhys. Lett. 83, 16004.
Henry, H., Levine, H., 2004. Dynamic instabilities of fracture under biaxial strain using a phase field model. Phys. Rev. Lett. 93, 105504.
Herring, C., 1951. in: Kingston, W.E. (Ed.), The Physics of Powder Metallurgy. McGraw-Hill, New York.
Hodgdon, J.A., Sethna, J.P., 1993. Derivation of a general 3-dimensional crack propagation law–a generalization of the principle of local symmetry. Phys. Rev. B 47, 4831–4840.
Hutchinson, J.W., Suo, Z., 1992. Mixed mode cracking in layered materials. Adv. Appl. Mech. 29, 63–191.
Irwin, G., 1957. J. Appl. Mech. 24, 361.
Karma, A., Lobkovsky, A., 2004. Unsteady crack motion and branching in a phase-field model of brittle fracture. Phys. Rev. Lett. 92, 245510.
Karma, A., Kessler, D., Levine, H., 2001. Phase-field model of mode III dynamic fracture. Phys. Rev. Lett. 8704, 045501.
Katzav, E., Adda-Bedia, M., Arias, R., 2007. Theory of dynamic crack branching in brittle materials. Int. J. Fract. 143, 245–271.
Landau, L.D., Lifshitz, E.M., 1975. The Classical Theory of Fields. Pergamon Press, Oxford.
Leblond, J., 2005. Private communication.
Marconi, V., Jagla, E., 2005. Diffuse interface approach to brittle fracture. Phys. Rev. E 71, 036110.
Marder, M., 2004a. Cracks cleave crystals. Europhys. Lett. 66 (3), 364–370.
Marder, M., 2004b. Effect of atoms on brittle fracture. Int. J. Fract. 130, 517–555.
Mumford, D., Shah, J., 1989. Optimal approximations by piecewise smooth functions and associated variational-problems. Commun. Pure Appl. Math. 42 (5), 577–685.
Noether, E., 1918. Invariante Variationsprobleme. Nachr. v. d. Ges. d. Wiss. zu Göttingen, pp. 235–257.
Oleaga, G., 2001. Remarks on a basic law for dynamic crack propagation. J. Mech. Phys. Solids 49 (10), 2273–2306.
Pons, A., Karma, A., 2008, in preparation.
Rice, J., 1968. A path independent integral and approximate analysis of strain concentration by notches and cracks. J. Appl. Mech. 35 (2), 379.
Sih, G., 1965. Stress distribution near internal crack tips for longitudinal shear problems. J. Appl. Mech. 32 (1), 51.
Sommer, E., 1969. Formation of fracture "lances" in glass. Eng. Fract. Mech. 1, 539–546.
Spatschek, R., Hartmann, M., Brener, E., Müller-Krumbhaar, H., Kassner, K., 2006. Phase field modeling of fast crack propagation. Phys. Rev. Lett. 96, 015502.
Wang, Y., Jin, Y., Khachaturyan, A., 2002. Phase field microelasticity theory and modeling of elastically and structurally inhomogeneous solid. J. Appl. Phys. 92 (3), 1351–1360.
William, M., 1957. On the stress distribution at the base of a stationary crack. J. Appl. Mech. 24, 109–114.